Physica Scripta

PAPER

Electronic, elastic, and thermodynamic properties of complex hydrides XAlSiH (X = Sr, Ca, and Ba) intended for hydrogen storage: an *ab-initio* study

RECEIVED
8 February 2024

REVISED
7 May 2024

ACCEPTED FOR PUBLICATION
14 May 2024

PUBLISHED
24 May 2024

H Ammi[1,2], **Z Charifi**[3,4,*], **H Baaziz**[3,4,*], **T Ghellab**[3,4], **L Bouhdjer**[1,2] **and S Adalla**[1,2]

[1] Department of Physics, Faculty of Sciences and Applied Sciences, University of Bouira, 10000 Bouira, Algeria
[2] Laboratory of Material Physics and Optoelectronic Compounds, University of Bouira, Algeria
[3] Department of Physics, Faculty of Science, University of M'sila, 28000 M'sila, Algeria
[4] Laboratory of Physics and Chemistry of Materials, University of M'sila, Algeria
[*] Authors to whom any correspondence should be addressed.

E-mail: charifizoulikha@gmail.com **and** baaziz_hakim@yahoo.fr

Keywords: hydrogen storage materials, thermodynamic and elastic properties, hydrogen desorption temperatures, anisotropy

Abstract

The mechanical and thermodynamic properties of polyanionic hydrides XAlSiH (X = Sr, Ca, and Ba) were evaluated using density functional theory (DFT). The thermal parameters of XAlSiH hydrides, such as the Grüneisen parameter γ, heat capacity, and thermal expansion coefficient, were computed for the first time. The quasi-harmonic Debye model was used to determine these parameters over a range of pressures (0–40 GPa) and temperatures (0–1000 K). The gravimetric hydrogen storage capacities for BaAlSiH, SrAlSiH, and CaAlSiH were found to be 0.52%, 0.71%, and 1.05%, respectively. The hydrogen desorption temperatures for these compounds were also simulated at 748.90 K, 311.57 K, and 685.40 K. Furthermore, semiconducting behavior with an indirect bandgap value between 0.2 and 0.7 eV was exhibited by these compounds using the GGA and LDA approximation, and between 0.7 and 1.2 eV using the mBJ-GGA and mBJ-LDA approximation. Accurate elastic constants for single crystals were obtained from the calculated stress–strain relationships. The elastic constants for the XAlSiH compounds were significantly higher than those for other hydrides. The [001] direction was more compressible than the [100] direction in the hexagonal structure of XAlSiH. A lower bulk modulus than metallic hydrides was exhibited by these materials, indicating that XAlSiH compounds (X = Sr, Ca, and Ba) were highly compressible. The melting temperature for CaAlSiH was higher than that for SrAlSiH and BaAlSiH. Consequently, the decomposition temperature for XAlSiH (X = Sr and Ba) at which hydrogen was released from a fuel cell was lower than that for CaAlSiH. The bonding behavior of CaAlSiH was more directional than that of SrAlSiH and BaAlSiH. Brittle materials were XAlSiH (X = Sr, Ca, and Ba). Our PBE calculations yield linear compressibility and orientation-dependent Young's modulus. Materials composed of hexagonal XAlSiH (where X represents Sr, Ca, or Ba elements) exhibit anisotropy in Young's modulus but isotropy in bulk modulus.

1. Introduction

In recent times, there has been extensive research on renewable energy sources as a result of the constraints posed by finite energy resources including oil, coal, and gasoline [1, 2]. The primary issue associated with utilizing renewable energy sources for powering automobiles is the inherent inefficiency of the processes involved [3, 4]. Hydrogen energy is considered a promising alternative due to its abundant and inexhaustible source [5–7]. Nevertheless, the direct compression of hydrogen gas into the tank resulted in suboptimal efficiency over extended periods of operation. The internal mechanisms involved in the storage of hydrogen in solid-state forms have been extensively investigated due to their exceptional gravimetric and volumetric energy

densities [8]. Hydrogen can undergo reversible storage and release from a host metal or complex hydrides via chemical processes [9, 10]. The remarkable hydrogen storing capacities of hydrides have sparked much curiosity. These hydrides have demonstrated improved hydrogen storage capabilities at lower temperatures and are also more economically efficient compared to traditional intermetallic hydrides.

Extensive research has been conducted on hydrides because of their potential as chemicals for storing hydrogen [10], their candidature for exhibiting superconducting [11], and their utilization as materials for semiconductors [12]. The hydrogen density in metal hydrides is exceptionally high, surpassing that of liquids and even solid hydrogen in some cases [13]. Hydrides are currently being extensively studied as potential materials for storing hydrogen. This is because they are lightweight, have a high hydrogen content, and possess high volumetric and gravimetric densities. Additionally, they exhibit excellent hydrogen absorption and desorption kinetics under operational conditions. In order to achieve effective hydrogen release without substantial heating, advantageous hydrides should have a high ratio of hydrogen to metal and should not be extremely stable. The compounds XAlSiH (X = Sr, Ca, and Ba) have been previously proposed as prospective candidates for high-temperature conductivity because of the arrangement of hydrogen atoms in their crystal structures, which could result in the creation of hydrogen-based conduction bands. An in-depth comprehension of the physical characteristics of hydrides plays a crucial role in the investigation and development of novel hydrogen storage compounds. While the structural and electronic characteristics of hydrides, specifically SrAlSiH [14], have been examined, there is currently no available information in the literature on their thermodynamic or elastic properties.

The total energy of XAlSiH (X = Sr, Ca, and Ba) hydrides was investigated and the findings are reported in this paper. The methodology for the theoretical calculations is outlined in section 2, whereas the findings of this study are based on density functional theory (DFT) and are reported in section 3. Specifically, the ground-state results at zero temperature for the XAlSiH (X = Sr, Ca, and Ba) hydrides are presented. Subsequently, conclusions are derived from our findings in section 4. The crystal structure and bonding of XAlSiH (X = Sr, Ca, and Ba) compounds were characterised and the electronic properties, including band structures and density of states (DOS), were examined. The thermal properties of the lattice were also computed, comprising entropy S, thermal expansion α, and specific heat at constant volume and pressure (C_v and C_p), which were derived using the Gibbs energy non-equilibrium. Furthermore, first-principle estimations of the elastic constants for XAlSiH (where X represents Sr, Ca, or Ba) are presented, along with comparisons of the hydrides' X–H distances, bulk moduli (B), and melting temperatures (T_m). By deriving a correlation between B and the melting temperature from the provided data, it becomes possible to make theoretical approximations regarding the decomposition temperature (T_d) when exposed to different conditions, including high pressure and the presence of catalysts. Furthermore, the elastic anisotropy and Debye temperatures of XAlSiH (X = Sr, Ca, and Ba) are examined.

2. Details of computation

The Full Potential Linearized Augmented Plane Wave (FP-LAPW) method with an approach based on the implementation of DFT in the WIEN2k code [15] was chosen for the first principles methods. To assess the exchange and correlation potential, we employed the Local Density Approximation (LDA) and the Generalized Gradient Approximation (GGA) [16].

The wave functions in the interstitial space were expanded by employing plane waves with a cut-off value of $k_{\max} \times$ R.M.T = 7.0, where R.M.T represents the radius of the Muffin-Tin sphere and $k_{\max}$ denotes the maximum vector of the plane wave. The charge density was expanded using Fourier analysis up to a maximum value of $G_{\max} = 16$ (Ryd)$^{1/2}$, and the valence wave functions within the MT spheres were expanded up to a maximum value of $l_{\max} = 10$. The energy difference between the core and valence states was set to −8.0 Ry for the current calculations. A convergence criterion of 10^{-4} Ry was implemented in order to attain self-consistent total energy. Furthermore, 1000 k points were employed for the purpose of sampling the first *Brillouin zone* (BZ).

Hamiltonian-type models (e.g. Mott-Hubbard or Anderson's impurity model) seem to be a more natural voice for dealing with highly correlated systems. The Mott-Hubbard model explicitly expresses the opposition between kinetic energy (which depends on the bandwidth defined by the jump integral t) and Coulomb repulsion U between electrons belonging to the same atom. The GGA+U method is a combination of the GGA approximation and this model: a correction is made locally, only on the d orbitals in the case in question, by introducing a Hubbard type term $\frac{1}{2}(U\sum_{i\neq j} n_i\, n_j)$. In our case, the atomic configuration of the elements constituents of our compounds is

Al: [Ne] 3 $s^2 3p^1$
Si: [Ne] 3 s^2 $3p^2$
H: $1s^1$

Sr: [Kr] $5s^2$
Ca: [Ar] 4 s^2
Ba: [Xe] $6s^2$

The *d* orbitals are occupied in the elements *Sr* and *Ba*, but in other cases only the *s* and *p* orbitals are present. Therefore, our system lacks strong correlation due to the absence of partially filled strongly correlated *d* or *f* electrons, which are typically involved in strong bonding.The properties of the minimum energy state were determined using a formalism based on DFT, when the temperature and pressure were reduced to absolute zero. To account for the influence of pressure, a factor (PV) is incorporated into the energy equation. On the other hand, the impact of temperature is represented by integrating the thermal contribution of the crystal's degrees of freedom in the free energy calculation. Crucial data for optimizing the production procedures and studying the future behavior of materials in their respective surroundings can be acquired. The Gibbs2 code, created by Blanco et *al* [17, 18], utilizes the quasi-harmonic Debye framework [19] to compute the thermodynamic properties of materials and consider temperature influences that were disregarded by the Born–Oppenheimer approach.

This program applies the quasi-harmonic Debye model to calculate the Debye temperature θ_D and the out-of-equilibrium Gibbs function $G^*(V, P, T)$. Furthermore, additional macroscopic characteristics associated with pressure and temperature can be ascertained using conventional thermodynamic equations. The Gibbs function, in a state of being out of equilibrium, assumes a particular form. In our study, we employ an out-of-equilibrium Gibbs free energy formulation denoted as $G^*(x,V;P,T)$, which captures the non-equilibrium behavior of the system under investigation. This formulation incorporates several key components that contribute to the overall free energy of the system [17, 18]. The equation is expressed as follows:

$$G^*(x,\ V;\ P,\ T) = E_{sta}(x,\ V) + PV + F^*_{vib}(x,\ V;\ T) + F^*_{el}(x,\ V;\ T) \tag{1}$$

x represents a relevant parameter of the system, such as composition or concentration, while V denotes the volume of the system. The term $E_{sta}(x,V)$ corresponds to the static energy of the system, which includes contributions from factors such as chemical composition and structural arrangement.

The second term, PV, represents the mechanical work done by the system against external pressure *P* as it undergoes volume changes *V*. This term accounts for the pressure-volume work in the overall free energy calculation. The vibrational term $F^*_{vib}(x,\ V;\ T)$ represents the contribution of thermal vibrations, such as phonons, to the free energy of the system. This term accounts for the energy associated with lattice vibrations and their interactions with other degrees of freedom. Similarly, the electronic term $F^*_{el}(x,\ V;\ T)$ captures the electronic contributions to the free energy, including effects such as electronic excitations and interactions between electrons and the crystal lattice. The electronic parts of free energy and entropy contribute three to four orders of magnitude less than the vibrational terms, and their impact on the calculated thermodynamic properties is negligible. They found that the electronic contribution to the Helmholtz free energy is extremely negligible for metals [17]. In our case, XAlSiH (where X = Sr, Ca, and Ba) are semiconductors. Unlike metals with partially occupied electron bands, these semiconductors have a significantly smaller electronic dependence on free energy due to their completely occupied electron bands. This guarantees the exclusion of the electronic component of the Helmholtz free energy ($F^*_{el}(x,\ V;\ T)$ term of equation (1)) from the calculations.By considering these various contributions, equation (1) provides a comprehensive framework for describing the non-equilibrium Gibbs free energy of the system, incorporating both static and dynamic factors that influence its energy state under varying conditions of pressure, temperature, and composition. The expression for this condition is as follows [20].

$$G(P,\ T) = \min_{x,V} G^*(x,\ V;\ P,\ T) \tag{2}$$

As a result, it is feasible to execute a Gibbs function minimization in accordance with volume V.

$$\frac{\partial G^*}{\partial V} = 0 = -P_{sta} + P - P_{th} \tag{3}$$

$P_{sta} = \partial E_{sta}/\partial V$ represents the static pressure, $P_{th} = \partial F^*_{vib}/\partial V$ signifies the thermal pressure, and *P* denotes the applied pressure. The thermal equation of state (EOS) is obtained through the resolution of equation (2). The quasi-harmonic approximation utilizes the density of vibrational states $g(\omega)$ to characterize the vibrational energy F^*_{vib}: (atomic units are used throughout the article):

$$F^*_{vib} = \int_0^\infty \left[\frac{\omega}{2} + k_B T \ln\left(1 - e^{-\omega/k_B T}\right)\right] g(\omega)\partial\omega \tag{4}$$

$$F^*(x,\ V;\ T) = E_{sta}(x,\ V) + F^*_{vib}(x,\ V;\ T) \tag{5}$$

The Debye model [21] is an approximation for the phonon spectrum that is frequently employed. The solid is regarded as a continuous and isotropic elastic medium, with its discontinuous corpuscular characteristics disregarded. The acoustic waves are the ones that propagate in this model devoid of dispersion. In a direct

proportionality to the wave vector, the frequencies vary. The *3p* phonon branches, where *p* is the number of basis atoms per primitive unit cell, are subsequently substituted with three acoustic branches in accordance with the equation $\omega = C_D k$, where C_D denotes the velocity of sound in the solid under consideration. It is necessary for the total number of vibration modes to be equal to $3pN$, where N is the number of primitive unit cells in the crystal. This constraint applies to the wave vector k_D, which corresponds to the radius of a sphere containing precisely n wave vectors. Consequently, the phonon state density assumes a quadratic form:

$$g_{Debye}(\omega) = \begin{cases} 9n\omega^2/\omega_D^3 & if \quad \omega < \omega_D \\ 0 & if \quad \omega \geqslant \omega_D \end{cases} \tag{6}$$

The variable n represents the density of unit cells in the crystal, expressed as $n = N/V$.

The Debye frequency, ω_D, is directly correlated with the Debye temperature.

$$\theta_D = \frac{\omega_D}{k_B} = \frac{1}{k_B}(6\pi^2 n)^{\frac{1}{3}}\nu_0 \tag{7}$$

ν_0 represents the average velocity across the three acoustic phonon branches, one longitudinal and two transverse.

The Grüneisen coefficient in quasi-harmonic model of Debye is defined as follows, with respect to the volume:

$$\gamma = -\frac{\partial ln\theta_D}{\partial lnV} \tag{8}$$

The thermodynamic properties derived by incorporating $g_{Debye}(\omega)$ into the quasi-harmonic formulas are as follows: The quantities of interest are Helmholtz's free energy (F), entropy (S), constant volume and pressure heat capacity (C_V and C_p), and thermal expansion coefficient α.

$$F = E_{sta}(x,\ V) + \frac{9}{8}nk_B\theta_D + 3nk_B Tln(1-e^{-\theta_D/T}) - nk_B TD\left(\frac{\theta_D}{T}\right) \tag{9}$$

$$S = -3nk_B ln(1 - e^{-\theta_D/T}) + 4nk_B D\left(\frac{\theta_D}{T}\right) \tag{10}$$

$$C_V = 12nk_B D(\theta_D/T) - \frac{9nk_B\theta_D/T}{e^{\theta_D/T} - 1} \tag{11}$$

$$C_p = C_v(1 + \alpha\gamma T) \tag{12}$$

$$\alpha = -\frac{1}{V}\left(\frac{\partial V}{\partial T}\right)_P = \frac{\gamma\ C_V}{B_T V} \tag{13}$$

The symbol B_T indicates the modulus of isothermal compressibility, the symbol n refers to the number of atoms per primitive cell, and the symbol D(x) symbolizes the Debye integral.

$$D(x) = \frac{3}{x^3}\int_0^x \frac{y^3 e^y}{1-e^y}\,\partial y \tag{14}$$

The elastic constants are computed using the IRELAST technique [22] which is included in the WIEN2k package.

3. Results and discussion

3.1. Structural properties

By covalently binding to the anionic substructure, hydrogen generates polyanionic hydrides. Five distinct structural categories are used to categorize the sixteen identified AeTrTt compounds (AlB_2, SrPtSb, $EuGe_2$, YPtAs, and $CaIn_2$): Ten of the nine electron ternary phases undergo isostructural arrangements and consist of ten electrons to produce charge-balanced quaternary polyanionic hydrides/deuterides. As a result of the additional electron supplied per formula unit by hydrogen, hydrogenation facilitates a more substantial transition from a metallic (or superconducting) to a semiconductor state, in addition to a minor geometric modification. The electronic density of states, where a band gap initiates at the Fermi level, manifests this transition in a conspicuous manner [23]. SrAlSiH was the initial quaternary polyanionic hydride to be investigated and documented in 2005 [24]. For a duration of 24 h, a particle comprising the precursor (SrAlSi) was immersed in a steel autoclave under conditions encompassing temperatures between 600 °C and 700 °C and an estimated 50 bars of hydrogen pressure. The particle maintained its integrity for the duration of the reaction. CaAlSiH was produced through the direct hydrogenation of CaAlSi at a pressure of 90 bars and a temperature of

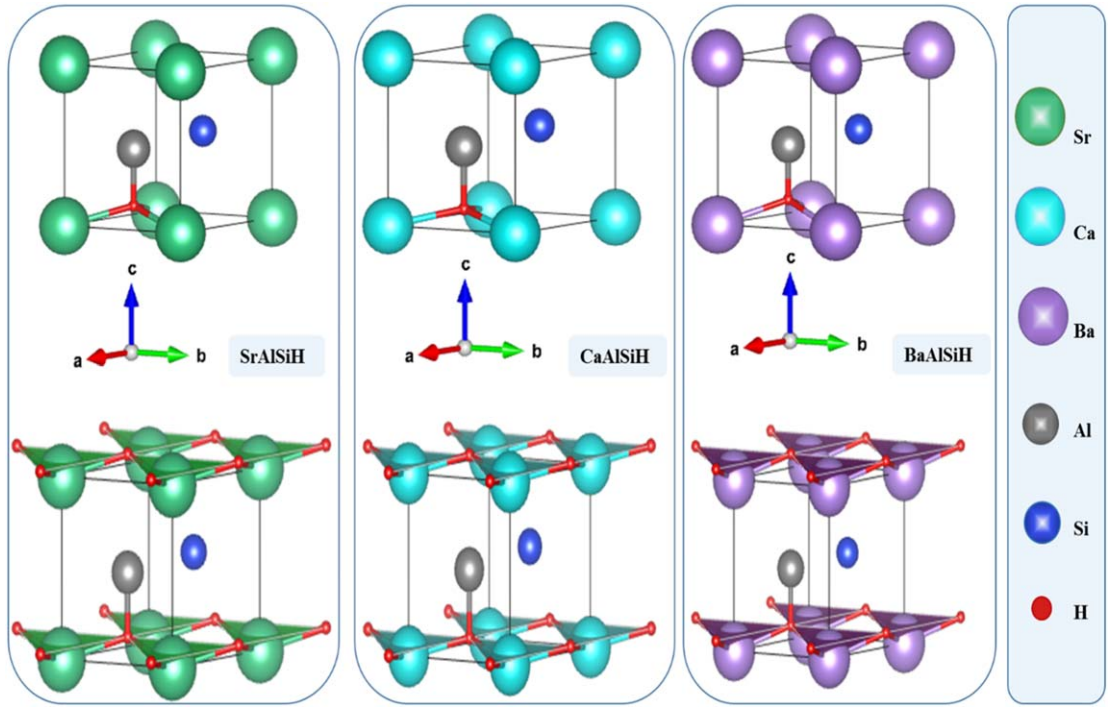

Figure 1. The crystal structure of XAlSiH (X = Sr, Ca, Ba).

Table 1. The atomic positions of XAlSiH (X = Sr, Ca, and Ba) with LDA and GGA.

Compounds	Atomic positions		Other calculation
	GGA	LDA	
SrAlSiH	Sr:0 0 0	Sr:0 0 0	Sr:(0 0 0) [26]
P3m1	Al:2/3 1/3 0.46024	Al:2/3 1/3 0.46024	Al:(2/3 1/3 0.5383) [26]
	Si:1/3 2/3 0.55455	Si:1/3 2/3 0,55455	Si:(1/3 2/3 0.4465) [26]
	H:2/3 1/3 0.10746	H:2/3 1/3 0.10746	H:(2/3 1/3 0.8970) [26]
CaAlSiH	Ca:0 0 0	Ca: 0 0 0	Ca:(0 0 0) [27]
P3m1	Al:2/3 1/3 0.45719	Al:2/3 1/3 0.45719	Al:(2/3 1/3 0.541) [27]
	Si:1/3 2/3 0.56597	Si:1/3 2/3 0.56597	Si:(1/3 2/3 0.446) [27]
	H:2/3 1/3 0.08385	H:2/3 1/3 0.08385	H: (2/3 1/3 0.893) [27]
BaAlSiH	Ba:0 0 0,00128	Ba:0 0 0	Ba:(0 0 0) [26]
P3m1	Al: 2/3 1/3 0,46447	Al:2/3 1/3 0,46481	Al:(2/3 1/3 0.5373) [26]
	Si: 1/3 2/3 0,54337	Si:1/3 2/3 0,54187	Si:(1/3 2/3 0.4568) [26]
	H: 2/3 1/3 0,13199	H:2/3 1/3 0,13447	H: (2/3 1/3 0.8637) [26]

500 °C for fifty minutes. BaAlSiH was similarly produced through the direct hydrogenation of BaAlSi at a temperature exceeding 600 °C and under a hydrogen pressure of 70 bars for a duration of two days.

This paper foxes into the crystal structure of technologically significant compounds known as Zintl phase hydrides, particularly the hydrides XAlSiH (X = Sr, Ca, or Ba). These hydrides fall under the category of Zintl phase hydrides, classified as quaternary polyanionic hydrides. A comprehensive study of the bonding and structure of these hydrides, as well as their stability, is necessary. Furthermore, the hexagonal phase of the XAlSiH (where X represents Sr, Ca, Ba) compounds was examined, specifically with space group (P3m1, No. 156) as shown in figure 1. This aligns remarkably well with the theoretical computations conducted by Myeong *et al* [14], and Björling *et al* [25], which forecast that XAlSiH undergoes crystallization in the hexagonal phase at lower temperatures. This study employed force optimization to achieve complete relaxation of hexagonal phase at different volume values, using both the local density approximation (LDA) and the generalized gradient approximation (GGA). The experimental data were juxtaposed with the anticipated atomic positions and are enumerated in table 1. The estimated results demonstrated a high level of concurrence with prior experimental investigations [26].

The total energy was computed by varying the volume of the unit cell, and then the Murnaghan equation of state was applied, [28] to fit the obtained data. Figure 2 displays the total energy as a variable of volume,

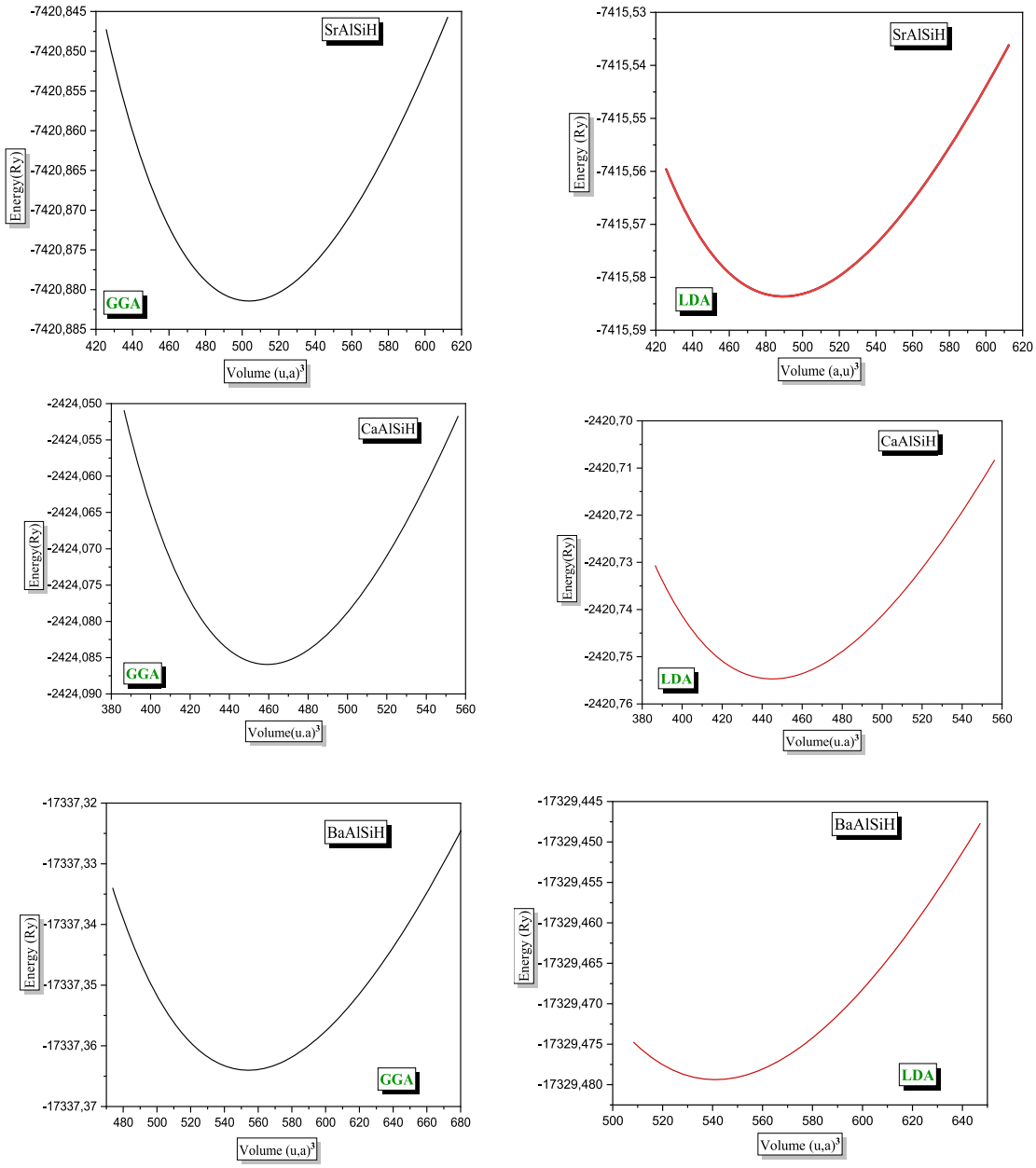

Figure 2. Variation of total energies as a function of volume of unit cell, using GGA and LDA for: XAlSiH (X = Sr, Ca, and Ba).

computed using the LDA and GGA approximations. Furthermore, the equilibrium lattice constants *a*, *b*, and *c*, as well as the bulk modulus (*B*) and their pressure derivatives (*B'*) for the XAlSiH (X = Sr, Ca, and Ba) compounds were determined. These values are listed in table 2 and are subsequently compared with the findings of earlier studies [25–27]. The lattice parameters we obtained closely match the values obtained through experimentation. The trend of decreasing bulk modulus from Ca to Sr to Ba is evident in the XAlSiH (X = Sr, Ca, Ba) compounds. Similarly, the unit cell volume, calculated using the LDA approximation, shows a gradual increase from 66.29 $Å^3$ to 72.89 $Å^3$ to 80.56 $Å^3$ as we move from the CaAlSiH structure to the SrAlSiH structure and finally to the BaAlSiH structure. The volume deviations, estimated using the GGA approximation, in comparison to the values provided by Björling *et al* [25], are 1.21%, 1.91%, and 3.77% for SrAlSiH, CaAlSiH, and BaAlSiH, respectively. The analysis of the structures of CaAlSiH, SrAlSiH, and BaAlSiH uncovers fascinating characteristics. Transitioning from Calcium to Barium, there is a noticeable expansion in cell size as the cell characteristics lengthen. This sequence demonstrates the ionic disparity among Ca^{2+}, Sr^{2+}, and Ba^{2+}.

The examined materials demonstrate a diminished bulk modulus the fundamental state phase when compared to metallic hydrides. This implies that the XAlSiH (where X represents Sr, Ca, and Ba) compounds are malleable, which signifies their high compressibility. In contrast to SrAlSiH and CaAlSiH compounds, BaAlSiH exhibits a significantly reduced in bulk modulus, which contributes to its greater equilibrium volume. As a result, BaAlSiH is the compound that is most readily compressible in comparison to the other compounds that

Table 2. Calculated lattice constants (*a*, *c* and *c/a*) in Å, bulk modulus (*B*) in GPa and pressure derivative (B′) at equilibrium volume using GGA and LDA compared to experimental findings of XAlSiH (X = Sr, Ca, and Ba) compound.

Compounds (structure type; space group)		Lattice Parameters			Relative error		
		GGA	LDA	Expt		GGA	LDA
SrAlSiH P3m1	***a***	4.193972	4.154385	4.2139 [50]/ 4.2113 [26]	$\nabla a/a\|_{Exp}$	−0.47/ −0.41	−1.43/ −1.36
	c	4.923202	4.876736	4.8902 [17]/ 4.9518 [60]	$\nabla c/c\|_{Exp}$	0.67/−0.58	−0.27/ −1.53
	c/a	1,162208	1,159262				
	B(Gpa)	61,7293	65,9613				
	B'	4,1250	4,3120				
	V(Å^3)	74.99	72.89	76.20 [6]	$\nabla V/V\|_{Exp}$	−1.61	2.80
CaAlSiH P3m1	***a***	4.113773	4.071890	4.1363 [26]/ 4.133 [61]	$\nabla a/a\|_{Exp}$	−0.54/ −0.46	−1.58/ −1.50
	c	4.664763	4.617271	4.7673 [26]/ 4.761 [62]	$\nabla c/c\|_{Exp}$	−2.19/ −2.06	−3.24/ −3.11
	c/a	1,133642	1,140051	1.1526 [27]			
	B(Gpa)	66,7257	71,4904				
	B'	3,9755	4,0003				
	V(Å^3)	68.36	66.29	70.27 [6]	$\nabla V/V\|_{Exp}$	−2.79	−6.00
BaAlSiH P3m1	***a***	4.281166	4.247193	4.3026 [63]/ 4.3087 [52]	$\nabla a/a\|_{Exp}$	−0.50/ −0.64	−1.30/ −1.44
	c	4.664763	5.156873	5.1441 [64]/ 5.1958 [26]	$\nabla c/c\|_{Exp}$	−0.10/ −0.11	0.24/−0.75
	c/a	1,208562	1,215843	1.2053 [27]			
	B(Gpa)	57,1437	61,4148				
	B'	4,2593	4,4983				
	V(Å^3)	74.04	80.56	84.12 [6]	$\nabla V/V\|_{Exp}$	−13.61	−4.41

Table 3. Calculated interatomic distances (Å) in XAlSiH (X = Sr, Ca, Ba) compounds.

	SrAlSiH			CaAlSiH			BaAlSiH		
	GGA	LDA	Expt	GGA	LDA	Expt	GGA	LDA	Expt
Al-Si (×3)	2.48632	2.48632	2.498 [65]	2.44611	2.44611	2.420 [59]	2.53657	2.53501	2.528 [59]
X-H(×3)	2.49945	2.49945	2.478 [65]	2.42435	2.42435	2.420 [59]	2.59518	2.60051	2.581 [59]
X-Si(×3)	3.29448	3.29448	3.237 [63]	3.14332	3.14332	3.246 [60]	3.47405	3.47482	3.413 [66]
X-Al(×3)	3.34422	3.34422	3.308 [59]	3.21498	3.21498	3.21 [65]	3.49336	3.49932	3.470 [66]
Al-H(×1)	1.75144	1.75144	1.768 [64]	1.75402	1.75402	1.75 [59]	1.74972	1.73842	1.73 [65]
Al-Si-Al(×3)	116.5388	116.5388	116.55 [24]	115.7548	115.7548	115.57 [24]	117.3752	117.4913	117.47 [24]
Si-Al-Si(×3)	116.5388	116.5388	116.55 [24]	115.7548	115.7548	115.57 [24]	117.3752	117.4913	117.47 [24]
Si-Al-H(×3)	100.8547	100.8547	100.83 [24]	102.0598	102.0598	102.33 [24]	99.4203	99.2052	99.25 [24]

were investigated. The gentle characteristics exhibits by the XAlSiH compounds (where X represents Sr, Ca, and Ba) result from a reduced strength of the bonding interaction among the X-Al, X-Si, and Al-Si elements. Moreover, as a result of their malleable nature, specific hydrogen atoms within the matrix can be perturbed, whereas Al–H bonds are typically strong.

Table 3 displays the interatomic distances found in the compounds SrAlSiH, CaAlSiH, and BaAlSiH. The distances between Al and H atoms in these compounds, known as XAlSiH, are very consistent, measuring roughly 1.75 Å. This uniformity persists regardless of the specific alkaline-earth metal present. The X-Al-Si-H lengths in XAlSiH are tightly grouped, with measurements of 2.4994 Å, 2.4243 Å, and 2.5951 Å, respectively. The values closely match the shortest X-H distances found in XH_2 salts with the cotunnite structure, especially for X = Sr and Ba [29, 30]. Nevertheless, the Ca-H distance in CaAlSiH is noticeably different from the smallest distances observed in CaH_2. These data support the notion of a covalent link existing between hydrogen and aluminum atoms. In addition, hydrogen atoms participate in ionic interactions with X atoms, resulting in an increase in the X-H distance from calcium to barium. The statistics shown in table 3 exhibit strong agreement with those derived from relaxed calculations of total energy. CaAlSiH and BaAlSiH compounds undergo hydrogen release when heated under vacuum conditions, starting at temperatures of around 420 °C and 500 °C, respectively. This release occurs by reversible reactions: $2CaAlSiH \leftrightarrow CaAlSi + H_2$ and $2BaAlSiH \leftrightarrow 2BaAlSi +$

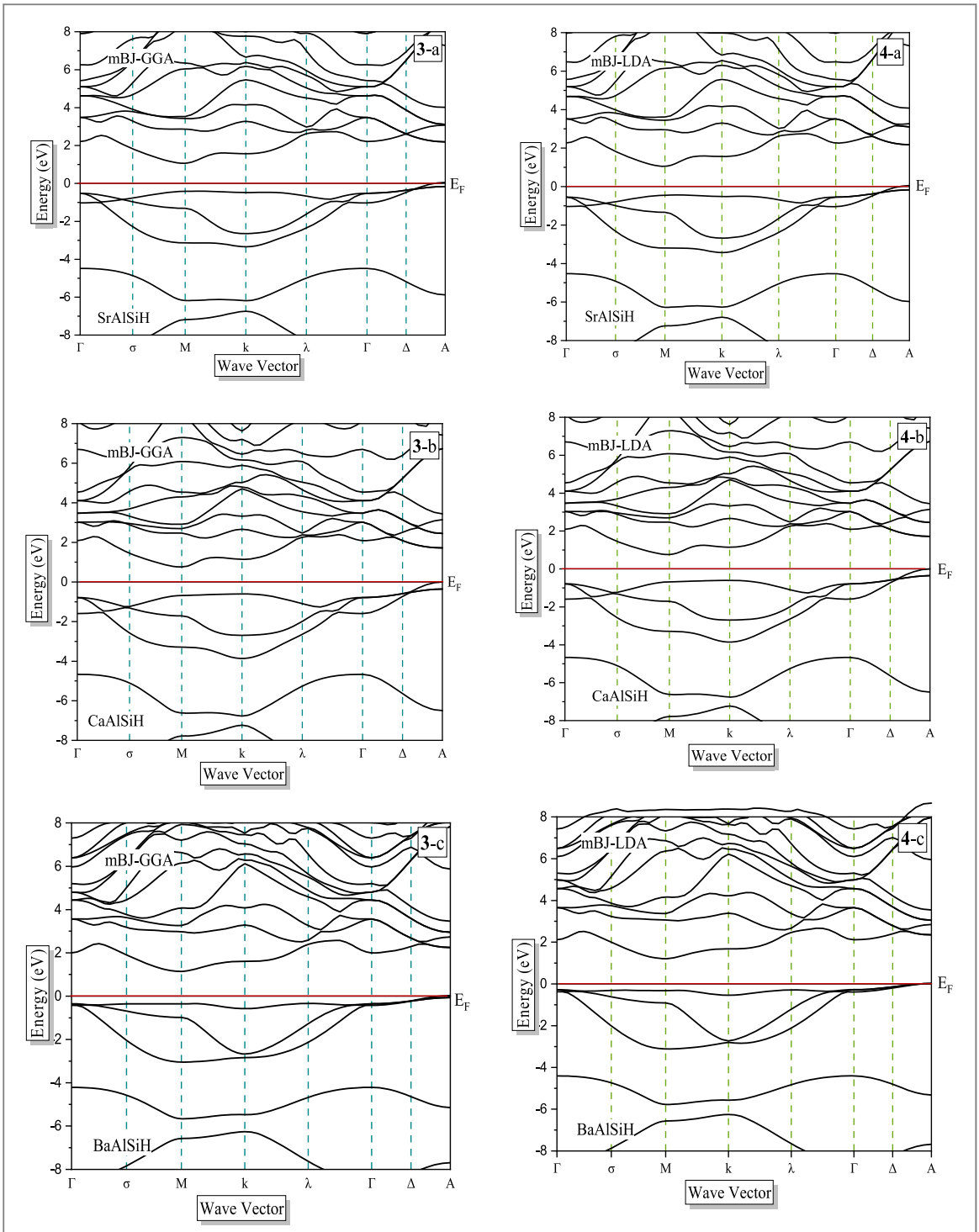

Figure 3. Band structure along the symmetry lines of the BZ for XAlSiH (X = Sr, Ca and Ba) (primitive Hexagonal; **P3m1**) using GGA (1-a,1-b,1-c), LDA(2-a,2-b,2-c), mBJ-GGA (3-a,3- b,3-c), and mBJ-LDA(4-a,4-b,4-c) approximations. (mBJ).

H_2. After undergoing dehydrogenation, the CaAlSi and BaAlSi alloys are restored. The decomposition temperature of CaAlSiH is lower than that of BaAlSiH and SrAlSiH, which present comparable decomposition temperatures. The decomposition temperature of BaH_2 and SrH_2 is 675 °C, but CaH_2 decomposes at a temperature below 600 °C [30]. The behavior of MAlSiH compounds demonstrates a similar pattern to that reported in AeH_2, emphasizing the significance of the M-H interaction in MAlSiH.

The calculation of relative error demonstrates that the deviation of the experimental lattice parameters according to GGA is lower than that according to LDA. As a result, the conclusion is reached that a solid approximation of the bonding of hydride properties is provided by GGA.

Table 4. Calculated E_g of XAlSiH (X = Sr, Ca, and Ba) compounds within GGA, LDA, and mBJ approximations.

Compounds	Band gaps (eV)				
	GGA	LDA	mBJ-GGA	mBJ-LDA	DFT
SrAlSiH (P3m1)	0.609	0,577	1.065	1.053	0.62 [31]
CaAlSiH (P3m1)	0.283	0,249	0.795	0.761	0.35 [31]
BaAlSiH (P3m1)	0.758	0,742	1.140	1.211	0.69 [31]

3.2. Electronic band structure and density of states

Figure 3 illustrates along different high-symmetry axes of the irreducible wedge of the *Brillouin zone* the energy bands of the XAlSiH (X = Si, Ca, and Ba) compounds, as determined by the GGA, LDA, mBJ-GGA, and mBJ-LDA methods. 'mBJ-GGA' stands for the modified Becke–Johnson Generalized Gradient Approximation, and 'mBJ-LDA' stands for the modified Becke–Johnson Local Density Approximation. These are modifications or corrections applied to standard DFT methods to improve their accuracy in describing certain electronic properties, especially for semiconductors and insulators. For the hexagonal phases of XAlSiH (X = Si, Ca, and Ba), the valence band reaches its maximum at point M, whereas the conduction band passes through its minimum in the σ-K direction. Thus, XAlSiH (X = Si, Ca, and Ba) possesses an indirect band gap M $\rightarrow$ σ-K and a band structure that is qualitatively identical. An indirect gap of 0.609 eV is acquired in the SrAlSiH compound via GGA computation and 0.577 eV with LDA. In comparison, the indirect band gaps of CaAlSiH and BaAlSiH are 0.283 eV and 0.249 eV, respectively, using the GGA approximation and 0.758 eV and 0.742 eV, respectively, using the LDA approximation. Based on the analysis of the diagrams, it can be determined that the separation between the valence and conduction bands spans a range of 0.2 eV to 0.7 eV. This considerably narrows the band gap, which endows the XAlSiH (X = Si, Ca, and Ba) compounds with notable conductivity. Table 4 summarizes the energy gap values obtained using different approximations.

According to earlier research [31], the obtained energy band gaps are sufficiently acceptable.

The previous values were refined under the influence of the mBJ-GGA and mBJ-LDA approximations. The mBJ-GGA approximations now stand at 1.065 eV, 0.795 eV, and 1.140 eV, respectively. As for the mBJ-LDA approximations, we obtained values of 1.053 eV, 0.76 eV, and 1.27 eV for SrAlSiH, CaAlSiH, and BaAlSiH, respectively.

The Total and partial Density of States (DOS) corresponding to the equilibrium volumes of the ground-state phases of XAlSiH (X = Si, Ca, and Ba) compounds are illustrated in figure 4. An extensive examination of the Total Density of States (DOS) curve in the investigation of XAlSiH compounds (where X represents Si, Ca, and Ba) reveals discernible characteristics in their valence bands in comparison to the SrAlSiH compound. The DOS curve reveals that there are two distinct regions within the valence band. The first region, which extends from −7.1 to −4.38 eV, is predominantly composed of hydrogen and silicon *s*-states, in addition to aluminium *s* and *p* states. These elements significantly influence the electronic configuration of the compound. The second region, which spans from −4.11 eV to the *Fermi* energy (E_F), is characterized by the abundance of hydrogen *s* states, silicon *p* states, and aluminum *p* states. The distinct segregation of silicon *s* and *p* phases is particularly conspicuous in this particular segment. An analogous observation can be made regarding the CaAlSiH compound. Additionally, the two valence band regions are discernible. The lower energy range, spanning from −10.8 eV to −7.45 eV, exhibits a significant impact from silicon s states, suggesting that this element makes a substantial contribution. Between −6.88 eV and E_F, the upper region is characterized by the presence of silicon *p* states, aluminum *p* states, and hydrogen *s* states. The unique characteristics of the s and p phases of silicon are clearly visible in this segment. With regard to the BaAlSiH compound, the examination of the DOS curve shows the presence of three discrete areas within the valence band. The initial two energy levels, which extend from −9.52 eV to −6.42 eV and −5.77 eV to −4 eV, respectively, are characterized by substantial contributions from the silicon and aluminum *s* states, in addition to the hydrogen *s* state. Between −3.21 eV and E_F, the third region is comprised of silicon *p* states, aluminum *p* states, and hydrogen *s* states.

To summarize, there are recurring patterns in the valence bands of XAlSiH (X = Si, Ca, and Ba) compounds. Significantly, the process of combining hydrogen states with silicon *s* and *p* orbitals is observed, along with a combined influence from silicon, aluminum, and hydrogen states in the conduction bands. In addition, silicon *p* orbitals and hydrogen states primarily affect the characteristics of valence bands close to the *Fermi* level. When examining the three compounds, it is clear that SrAlSiH and CaAlSiH exhibit a decrease in the difference between the lowest and highest valence bands. This could have important consequences for their electronic properties. Each of these hydrides displays a limited range of energy levels between the valence and conduction

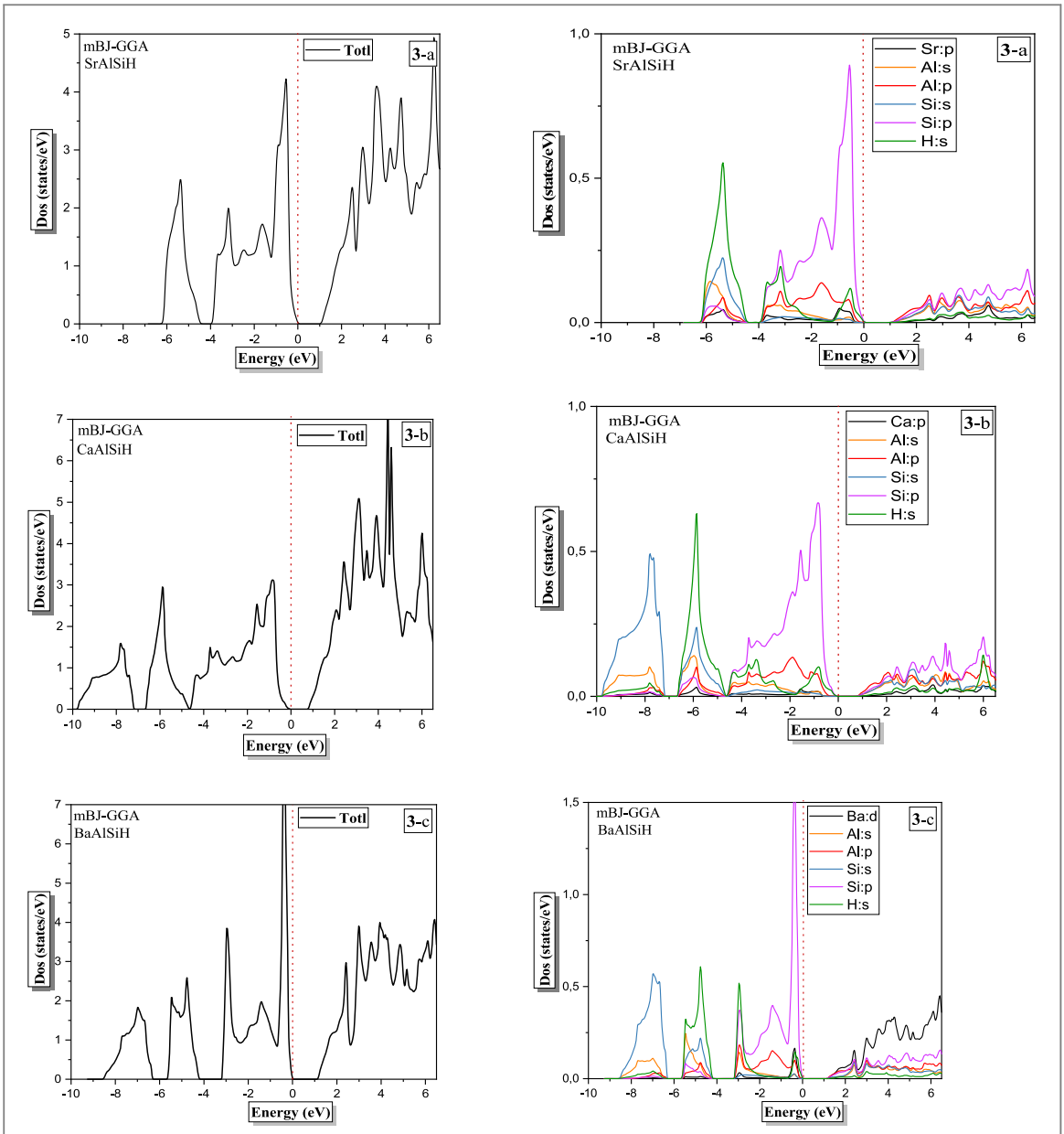

Figure 4. The calculated total and partial DOS for XAlSiH (X = Sr, Ca and Ba), using GGA (1-a,1-b,1-c), LDA(2-a,2-b,2-c), mBJ-GGA (3-a,3-b,3-c), and mBJ-LDA(4-a,4-b,4-c) approximations. (mBJ).

bands. Therefore, it is logical to infer that the CaAlSiH and BaAlSiH compounds function as semiconductors, akin to the previously examined SrAlSiH system. The band gap widths of BaAlSiH and CaAlSiH are 0.71 eV and 0.42 eV, respectively, in comparison to 0.65 eV for SrAlSiH [32]. The DOS curves for XAlSiD compounds (where X stands for Ca, Sr, and Ba) show a clear singularity that is a little below the Fermi level [27].

3.3. Thermodynamic properties

The thermodynamic properties of materials, such as thermal capacity, thermal conductivity, thermal expansion, and the Grüneisen parameter, are vital for understanding thermodynamic stability, atomic interactions, lattice vibration anharmonicity, and the potential applications of materials in different fields. Analyzing the changes in entropy (S), heat capacity (C_v), and Debye temperature (θ_D) in response to variations in pressure and temperature will greatly enhance our comprehension of the thermodynamic properties of XAlSiH hydrides (X = Sr, Ca, and Ba). In order to achieve this objective, ab-initio calculations are performed using a quasi-harmonic method, taking into account the influence of phonon effects throughout a temperature range from 0 to 1000 K. Furthermore, the evaluation of pressure's influence is conducted within the range of 0 to 40 GPa. This technology allows for a comprehensive investigation of the thermal characteristics of these intricate materials.

The predicted equilibrium volumes at various pressure levels and temperatures are depicted in figure 5. When heated, the total volume of our crystals expands. The volume variation of the compounds SrAlSiH,

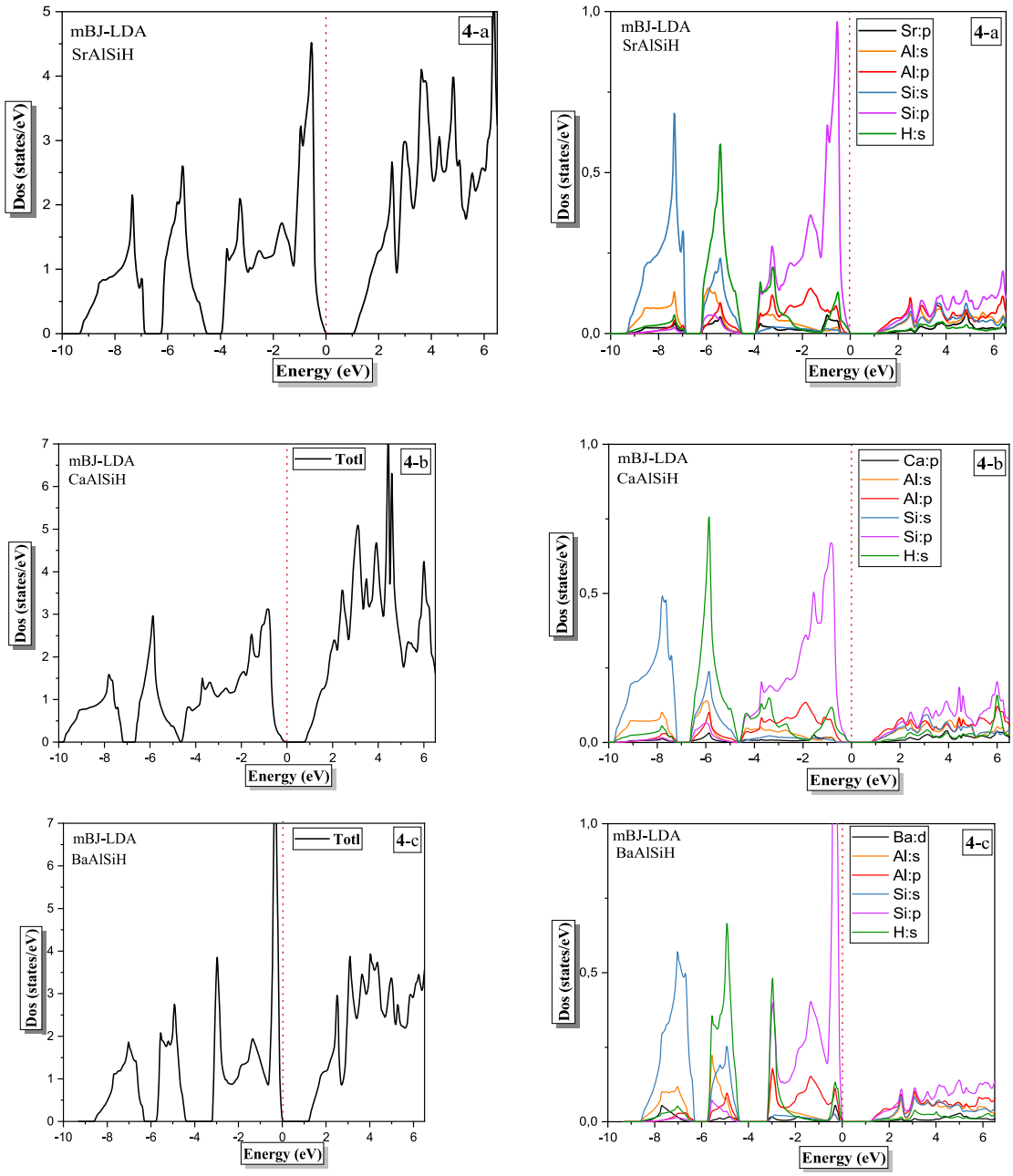

Figure 4. (Continued.)

CaAlSiH, and BaAlSiH follows a comparable pattern with respect to temperature. Furthermore, it is observed that the equilibrium volume of these compounds expands with increasing temperature, specifically when subjected to a pressure of 0 GPa, which indicates their nature as flexible materials.

The bulk modulus remains relatively stable between 0 and 200 K, followed by a linear decrease with increasing temperature, indicating an elevated compressibility with rising temperature (see figure 6). The calculated bulk modulus values are 70.03 GPa for CaAlSiH, 56.23 GPa for BaAlSiH, and 60.96 GPa for SrAlSiH at 0 K, aligning closely with our results 71,49 GPa, 66,72 GPa, and 57.14 GPa respectively using GGA obtained using the EOS method. These calculated bulk modulus values illustrate that CaAlSiH exhibits the least compressibility, followed by BaAlSiH, and then SiAlSiH at each pressure point. There is a consistent decline in bulk modulus as temperature increases, signifying an increase in compressibility at elevated temperatures. The bulk modulus of our compounds linearly increases with temperature, indicating a comparable change in cell volume.

The differentiation between the low- and high-temperature states of a crystal is determined by a physical property called θ_D. When the temperature surpasses the Debye temperature (θ_D), it is expected that all modes

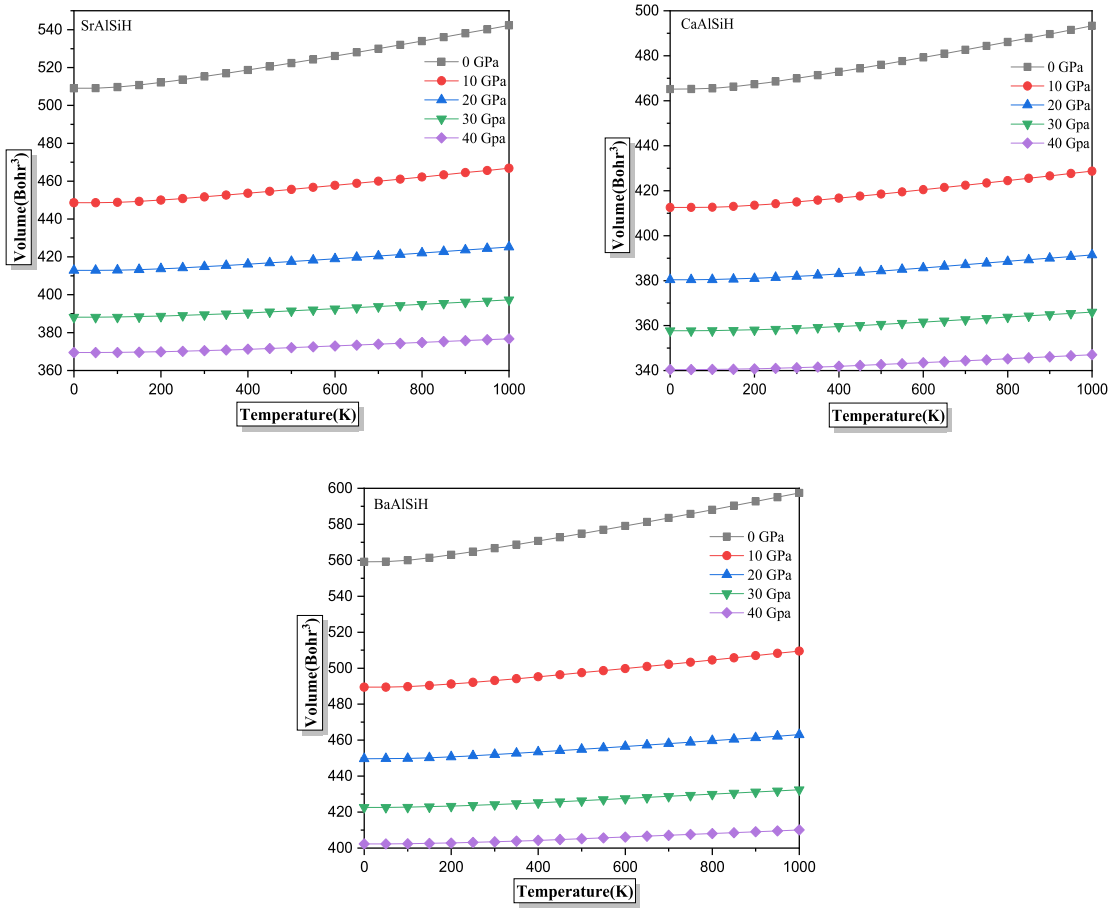

Figure 5. Variation of the cell volume as a function of temperature of XAlSiH (X = Sr, Ca, Ba) at different pressures calculated by GGA.

will possess an energy equivalent to k_BT. Conversely, a reduction in temperature below θ_D results in the solidification of high-frequency modes [33]. Figure 7 displays the temperature-dependent θ_D for XSiAlH (where X represents Sr, Ca, and Ba) at different pressures. The θ_D value is indicative of the strength of interatomic bonds and, thus, is correlated with the hardness of the material. In general, a larger θ_D indicates increased hardness. Nevertheless, the SrAlSiH, CaAlSiH, and BaAlSiH crystals exhibit a decrease in hardness when subjected to no pressure, a phenomenon that can be counteracted by the application of pressure, as evidenced by the correlation between the Debye temperature θ_D and temperature. The Debye temperatures θ_D for SrAlSiH, CaAlSiH, and BaAlSiH are 414.94 K, 518.05 K, and 350.08 K, respectively. These values were obtained at a temperature of zero K and a pressure of zero GPa for these compounds. The Debye temperature of a solid is often higher when it possesses a high modulus and hardness. These findings provide evidence for the adaptable characteristics of XSiAlH compounds and their mean Debye temperature. The Debye temperature demonstrates a progressive drop from 0 to 1000 K under conditions of low pressure. However, at a specific temperature, it escalates in conjunction with pressure. Hence, we might infer that pressure exerts a more pronounced influence on the Debye temperature θ_D compared to temperature.

The thermal capacity of a substance can be determined by analyzing its vibrational properties through thermodynamic measures such as heat capacity. Figures 8 and 9 illustrate the values of specific heat capacities under constant pressure and constant volume conditions, respectively. Regrettably, there are no previous outcomes available for comparison. Figure 8 clearly demonstrates that temperature has a considerably more pronounced effect on C_p than pressure, as can be easily recognized. Instead of being controlled by C_p heat capacity curves, these curves adhere to the classical Dulong and Petit law. The equipartition theorem of classical mechanics states that the kinetic and potential energy of each atom is precisely proportional to its three atomic degrees of freedom. Reference [34] states that there is a direct correlation between C_v and T^3 at low temperatures. When considering quantum oscillators as collective modes, known as phonons, in materials, it can be shown that only low-energy acoustic modes may be stimulated at low temperatures. At elevated temperatures, a direct correlation with temperature is observed. Temperatures over 250 K, where C_p is greater than C_v, indicate the thermodynamic stability of the crystal. Under conditions of zero pressure and room temperature, the specific

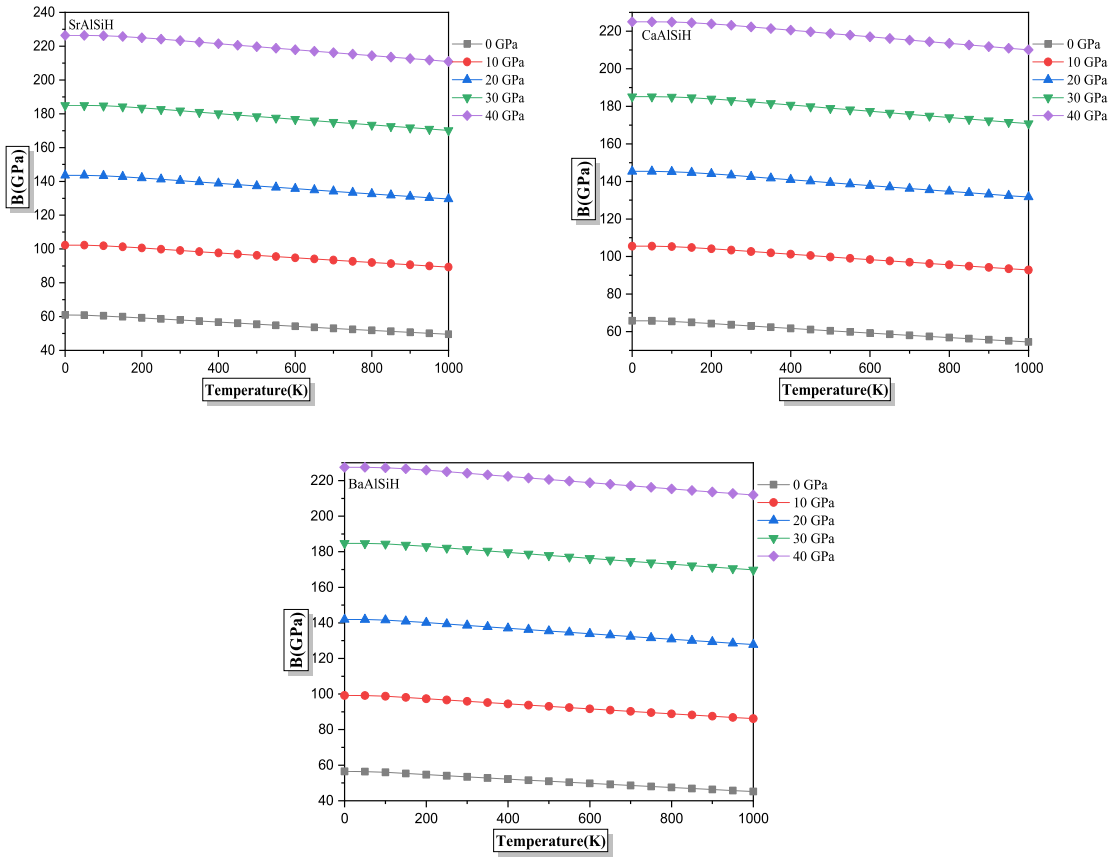

Figure 6. Variation of the bulk modulus as a function of temperature of XAlSiH (X = Sr, Ca, Ba) at different pressures calculated by LDA.

heat capacities C_v (Cp) for BaAlSiH, CaAlSiH, and SrAlSiH are 90.06 (104.51), 95.27 (100.78), and 96.68 (102.78) J mol^{-1} K^{-1}, respectively.

On a microscopic scale, entropy, represented by the symbol S, quantifies the level of disorder in a material. It can be proven that when temperature and pressure increase, entropy also increases. Although C_v is not affected by pressure, the entropy S shows a strong correlation with temperature (figure 10).

An additional noteworthy parameter is the thermal expansion coefficient (also known as volume expansion), represented by α. This value signifies the capacity of a substance to undergo volumetric changes as a result of fluctuations in temperature. It is critical to acknowledge that the assessment of the thermal expansion coefficient at elevated temperatures poses distinct difficulties that may result in substantial discrepancies in experimental findings [35]. Real substances are characterized by non-harmonic interactions among their atoms, which induce variations in potential energy as the interatomic separation increases. The increased activation of phonons with rising temperatures emphasizes the consequences of anharmonicity. As a consequence, the equilibrium separation of atoms is altered, which in turn causes the expansion of the lattice. Anharmonicity, or the asymmetrical dependence of potential energy on atomic separation, is the cause of this thermal expansion. Consequently, the thermal expansion coefficient ought to exhibit a temperature-dependent variation comparable to that of the heat capacity. Figure 11 represents the relationship between temperature and pressure and how it affects the thermal expansion coefficients of XAlSiH (X = Sr, Ca, and Ba). The graph shows that there is a linear correlation between temperature and thermal expansion coefficients within the range of 300 to 1000 K, after a sharp increase up to 300 K. Furthermore, evidence suggests that the coefficient reduces as pressure rises. The influence of temperature is less noticeable under low pressure and high temperature, suggesting that anharmonic effects play a more substantial role in the behavior of the tested materials under these circumstances. The thermal characteristics of SrAlSiH, CaAlSiH, and BaAlSiH at 0 GPa and room temperature are approximately 7.83×10^{-5} K^{-1}, 7.48×10^{-5} K^{-1}, and 8.04×10^{-5} K^{-1}, respectively. Ultimately, our findings underscore a notable resemblance among the three substances.

3.3.1. Hydrogen storage properties

An investigation was conducted on the hydrogen storage capabilities of the hydrides XAlSiH (X = Sr, Ca, and Ba). The gravimetric storage of hydrogen capacity, expressed as a percentage of the weight of material (Cwt %), is

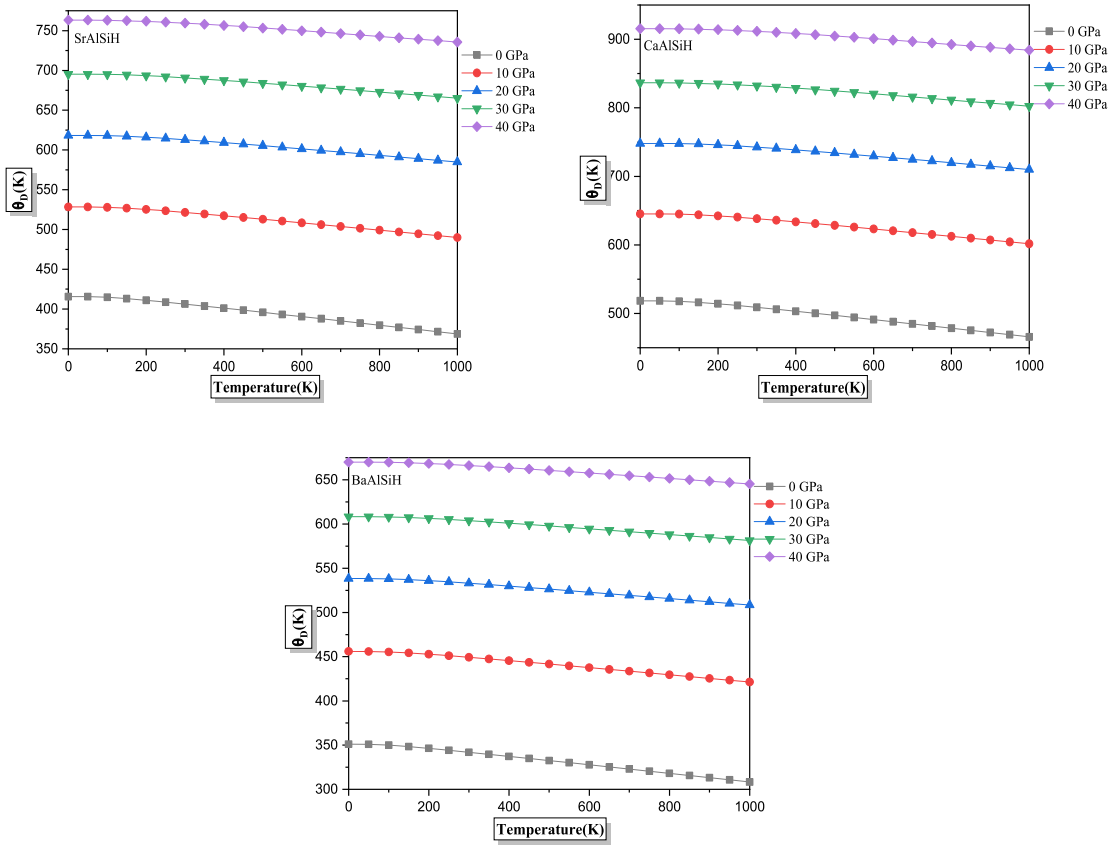

Figure 7. Variation of the Debye temperature θ_D as a function of temperature of XAlSiH (X = Sr, Ca, and Ba) at different pressures calculated by GGA.

a critical factor in hydrogen storage applications. It quantifies the quantity of hydrogen that can be stored per unit mass of a solid. Hence, its determination holds great significance for practical applications. The capacity for storing hydrogen gravimetrically can be determined by utilizing equation (15) [36].

$$CW\% = \left(\frac{\left(\frac{H}{M}\right) M_H}{M_{Host} + \left(\frac{H}{M}\right) M_H} \times 100 \right)\% \tag{15}$$

H represents the mass of hydrogen stored in the material, typically measured in grams. M denotes the total mass of the material, including both the hydrogen and the host material, also typically measured in grams. M_H is the molar mass of hydrogen, typically given in grams per mole. M_{Host} denotes the molar mass of the host material excluding hydrogen, also given in grams per mole.

The term 'H/M' denotes the atom ratio of hydrogen to material, which is the ratio of the number of hydrogen atoms to the number of atoms in the material. It represents the fraction of the material's composition that is hydrogen.

Cwt% represents the weight percentage of hydrogen stored within the material. H/M represents the atom ratio of hydrogen to material, as explained above. The equation calculates the weight percentage of hydrogen stored within the material by considering the ratio of hydrogen to the total material and adjusting for the molar masses of hydrogen and the host material. By plugging in the appropriate values for H, M, MH, and M_{Host} into this equation, one can calculate the weight percentage of hydrogen stored within the material. This equation is crucial for evaluating the gravimetric storing capacity of hydrogen in a given material [36].

The weight-based gravimetric hydrogen storage capacities for BaAlSiH, SrAlSiH, and CaAlSiH are determined to be 0.52%, 0.71%, and 1.05%, respectively.

Desorption temperature T_D is the second critical thermodynamic factor to consider when selecting a material for hydrogen storage. The temperature of our hydrides can be determined directly using the standard Gibbs equation (16) in the following manner:

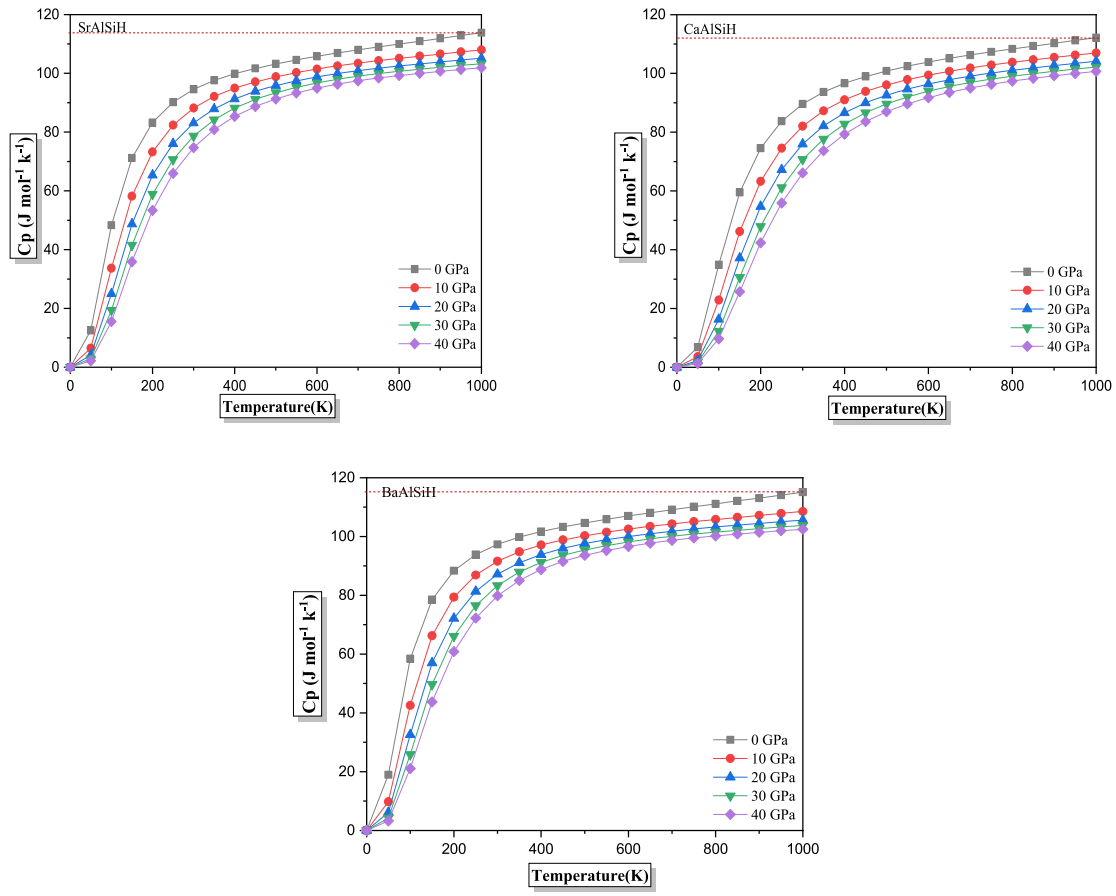

Figure 8. Variation of the heat capacity C_p versus temperature of XAlSiH (X = Sr, Ca, and Ba) at different pressures calculated by GGA.

$$\Delta G = \Delta H - T\Delta S \tag{16}$$

ΔG, ΔH, and ΔS represent, respectively, the standard Gibbs energy, enthalpy of formation, and entropy change of the dehydrogenation reaction. At equilibrium, the conventional Gibbs energy (ΔG = 0) is zero. The dehydrogenation temperature can subsequently be calculated using the subsequent formula:

$$T_D = \frac{\Delta H}{\Delta S} \tag{17}$$

For SrAlSiH, CaAlSiH, and BaAlSiH, ΔS corresponds to entropy changes of 134.73 J/mol.K, 105.72 J/mol.K, and 63.97 J/mol.K, respectively [37]. Thus, the temperatures at which hydrogen desorption occurs are determined to be 748.90 K, 311.57 K, and 685.40 K, in that order.

3.4. Elastic properties

Elastic constants serve to establish a correlation between the mechanical and dynamic properties of solids. Furthermore, they elucidate the characteristics of forces present within crystals as well as the inflexibility and durability of crystalline materials. The utilization of potential functions of the first and second orders is widespread in expressing forces and elastic constants, necessitating accurate techniques for their *ab initio* computations. Though, information regarding monocrystalline elastic constants is limited to a small number of instances [38]. Efforts have been undertaken to theoretically ascertain these constants using *ab initio* calculations. However, there is currently a lack of experimental and theoretical findings on elastic constants. Hexagonal systems have six unique elastic constants, namely C_{11}, C_{12}, C_{13}, C_{33}, C_{44}, and C_{66}. In order to acquire precise values for these elastic constants, it is imperative to comprehend the relationship between energy and stress for certain deformations. Deformations are selected to optimize the symmetry of the systems when subjected to stress. The WIEN2K package includes a feature that streamlines the process of optimizing internal cell design by utilizing force-driven optimization.

The stress–strain technique is employed to calculate the elastic constants C_{ij} utilizing the GGA approximation, as presented in table 5. The positive values of the elastic constants for the hexagonal crystals

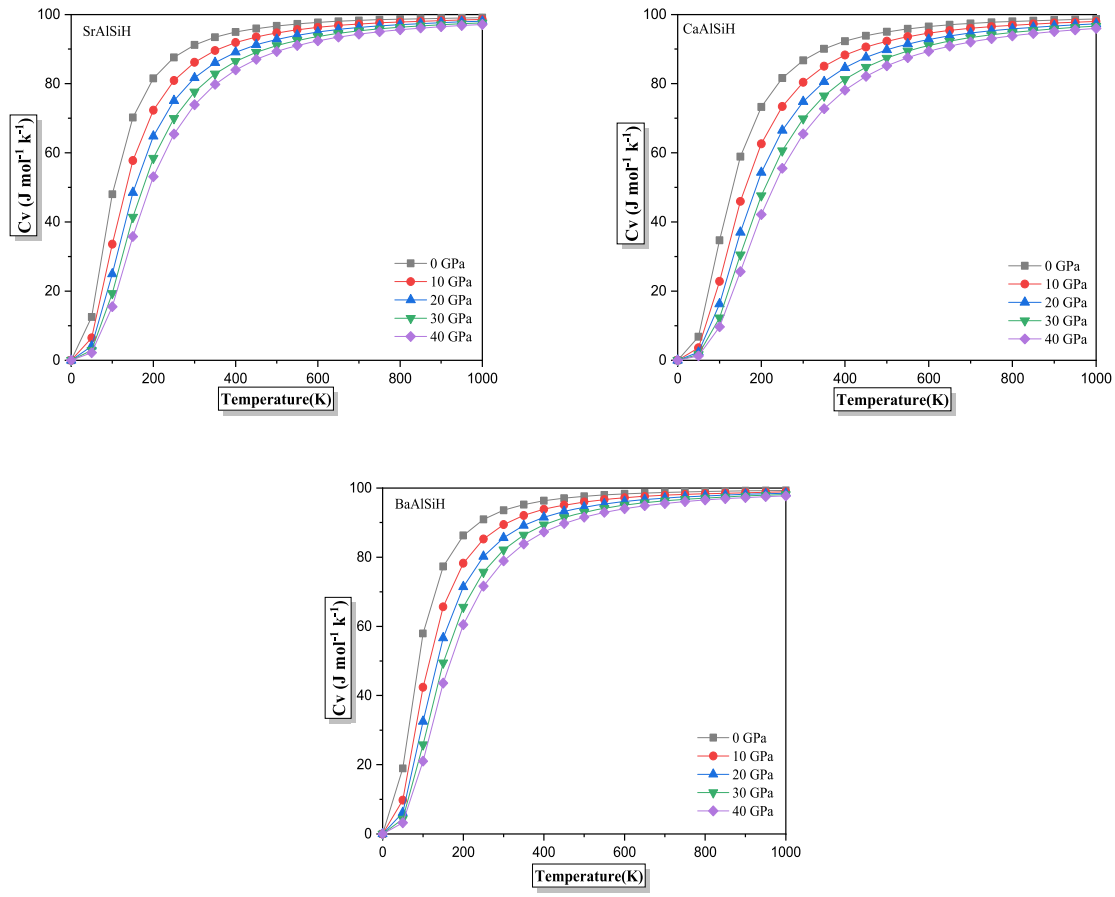

Figure 9. Variation of the heat capacity C_v versus temperature of XAlSiH (X = Sr, Ca, Ba) at different pressures calculated by GGA.

XAlSiH (X = Sr, Ca, and Ba) prove their mechanical stability. Therefore, we can confidently deduce that these compounds possess elastic stability, as they satisfy the following criteria:

$$\begin{aligned} &C_{44} > 0,\ C_{66} > 0,\ C_{11} > |C_{12}| \\ &C_{11}C_{33} > C_{13}^2 \\ &(C_{11} + C_{12})C_{33} - 2C_{13}^2 > 0 \end{aligned} \tag{17a}$$

Table 5 demonstrates that the elastic constants exhibit an ascending order of magnitude: C_{ij}(CaAlSiH) > C_{ij} (SrAlSiH) > C_{ij} (BaAlSiH). The obtained calculations indicate that the elastic constant C_{11} displays a greater value compared to the other constants. This observation implies that the XAlSiH hydrides exhibit greater resistance to alterations in shape and volume compared to alterations in length or volume. According to this idea, the ⟨100⟩ directions have the highest degree of packing density. Each compound has more compressibility along the *c*-axis compared to the a-axis, as indicated by the bigger value of C_{11} relative to C_{33}. Furthermore, C_{44} appears a smaller magnitude compared to C_{66}, suggesting that shear deformation is more readily achievable in the (001) plane as opposed to the (100) plane.

Hydrogen decomposition temperatures can be approximated using the melting points of XAlSiH (where X represents Si, Ca, or Ba), whereas the bulk modulus provides insight into the nature of the crystal bonds. $T_m = 607 + 9.3 \times B$ represents the correlation that Fine *et al* [39] found. Established between the elastic constants and the melting temperatures of metals and intermetallic materials [40, 41].

The attained result indicates a comparable correlation. Where, CaAlSiH (T_m = 1214.75 K) > SrAlSiH (T_m = 1206.55 K) > BaAlSiH (T_m = 1142.63 K) reveals a melting temperature trend that is at least equivalent to that of CaAlSiH (B = 65.35 GPa) > SrAlSiH (B = 64.468 GPa) > BaAlSiH (B = 57.59 GPa). BaAlSiH is anticipated to decompose at a lower temperature than the compounds CaAlSiH and SrAlSiH.

The Hill model [42, 43], was employed to estimate the shear modulus G and bulk modulus B by computing the arithmetic mean of the Voigt [44] and Reuss [45] models. Specific to a hexagonal system are the subsequent values for the Voigt shear modulus G_v, Voigt bulk modulus B_v, Reuss shear modulus G_R, and Reuss bulk modulus B_R, Hill bulk modulus B_H and Hill shear modulus G_H:

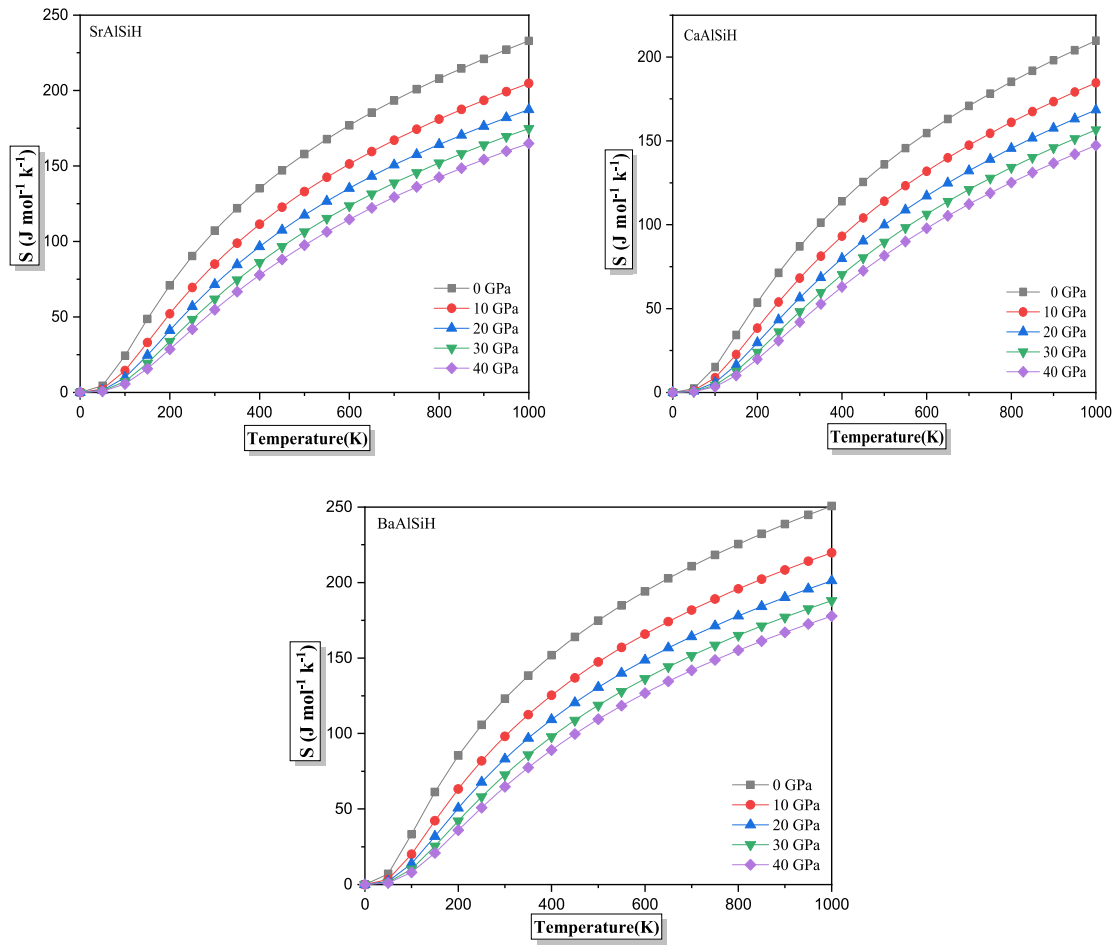

Figure 10. Variation of the entropy as a function of temperature of XAlSiH (X = Sr, Ca, Ba) at different pressures calculated by GGA.

$$B_V = \frac{2C_{11} + 2C_{12} + 4C_{13} + C_{33}}{9} \tag{18}$$

$$B_R = \frac{(C_{11} + C_{12})C_{33} - 2C_{13}^2}{C_{11} + C_{12} - 4C_{13} + 2C_{33}} \tag{19}$$

$$G_V = \frac{4C_{11} + 2C_{33} - 4C_{13} - 2C_{12} + 12C_{44} + 6C_{66}}{30} \tag{20}$$

$$G_R = 15\left(\frac{4C_{11} + 4C_{12} + 8C_{13} + 2C_{33}}{(C_{11} + C_{12})C_{33} - 2C_{13}^2} + \frac{6}{C_{11} - C_{12}} + \frac{6}{C_{44}} + \frac{3}{C_{66}}\right)^{-1} \tag{21}$$

$$B_H = \frac{1}{2}(B_V + B_R) \tag{22}$$

$$G_H = \frac{1}{2}(G_V + G_R) \tag{23}$$

The Voigt and Reuss models represent two extreme cases of elastic behavior in composite materials. The Voigt model assumes that the composite material behaves as if it were a single homogeneous material with uniform properties. In contrast, the Reuss model assumes that the composite material behaves as if it were a collection of independent materials with different properties. The Voigt and Reuss limits provide upper and lower bounds, respectively, for the bulk and shear moduli of composite materials. However, in practice, composite materials often exhibit behavior that falls between these two extremes. This is where the Hill model comes into play. The Hill model takes an average approach, considering both the Voigt and Reuss limits. It provides an effective means of estimating the overall elastic behavior of composite materials by averaging the results from the Voigt and Reuss models. The 'average' concept used in equation (22) for B_H and (23) for G_H stems from this approach. By averaging the results obtained from the Voigt and Reuss models, the Hill model provides a more realistic estimate of the elastic properties of composite materials.

Table 5. The elastic constants for XAlSiH (X = Sr, Ca, Ba) computed using GGA and melting temperature T_m (in K).

	SrAlSiH P3m1	CaAlSiH P3m1	BaAlSiH P3m1
C_{11}	163.2624	175.6237	143.4263
C_{33}	97.4601	94.061	92.2957
C_{44}	46.2550	43.1177	44.5489
C_{66}	65.3364	68.25125	59.02235
C_{12}	32.5895	39.1212	25.3816
C_{13}	27.2531	23.7807	24.7456
T_m	1206.5524 ± 300	1214.755 ± 300	1142.6335 ± 300
A_1	0.8972	0.7764	0.9568
A_2	1	1	1

The equations provided below are utilized in order to compute the modulus of Young E and the Poisson ratio σ [46]:

$$\begin{cases} E = \dfrac{9BG}{(G + 3B)} \\ \sigma = \dfrac{3B-2G}{2(3B + G)} = \dfrac{1}{2}\left(1 - \dfrac{E}{3B}\right) \end{cases} \tag{23a}$$

Reference [47] demonstrates that all XAlSiH (X = Sr, Ca, and Ba) materials appear strong compressibility, with their elastic parameters significantly lower than those of common metals [48] and intermetallic materials [49]. These findings suggest that all XAlSiH materials (where X represents Sr, Ca, and Ba) denote a significant degree of compressibility.

The compound SrAlSiH has a higher bulk modulus than BaAlSiH and CaAlSiH. For instance, B_V (CaAlSiH) = 68.74 GPa > B_V (SrAlSiH) = 66.46 GPa > B_V (CaAlSiH) = 31.43 GPa, suggesting that CaAlSiH has stronger bonding compared to SrAlSiH and BaAlSiH (see table 6). Table 2 displays that $d_{Ca\text{-}H}$ (CaAlSiH) = 1 Å < $d_{Ba\text{-}H}$ (BaAlSiH) = 2 Å < $d_{Sr\text{-}H}$ (SrAlSiH) = 3 Å. This provides substantial evidence in favor of the beginning hypotheses. Pugh [50] suggested that the ratio of shear moduli (B/G) of polycrystalline phases can be used as an indicator of ductility. In this context, shear modulus G reflects the ability to resist plastic deformation, whereas bulk modulus indicates resistance to fracture. A higher B/G ratio indicates increased ductility, with the crucial threshold for distinguishing ductile from fragile substances being 1.75. All our XAlSiH compounds (where X represents Sr, Ca, and Ba) exhibit brittleness.

The modulus Young E is an essential metric for the stiffness of a material, which is the ratio of stress to deformation under uniaxial tension or compression. In the transition from CaAlSiH to SrAlSiH and further to BaAlSiH, there is a consistent decrease in rigidity, indicating a reduction in the same direction for these systems. Notably, CaAlSiH displays greater resistance to unidirectional compression and tension compared to CaAlSiH and BaAlSiH; for instance, E_H (CaAlSiH) = 129.89 GPa > E_H (SrAlSiH) = 127.528 GPa > E_H (BaAlSiH) = 116.69 GPa (see table 6).

In the case of uniaxial deformation, the volume change is directly proportional to Poisson's ratio σ. When σ is less than 0.5, there is no volume change during elastic deformation, but when σ is low for XAlSiH materials (where X = Sr, Ca, and Ba), there are noticeable changes in volume. The values of σ_H (0.16 for BaAlSiH and 0.17 for SrAlSiH) are smaller than σ_H (0.18 for CaAlSiH), suggesting that BaAlSiH and SrAlSiH experience more pronounced volume changes during uniaxial deformation. In addition, no other elastic constant provides a more profound understanding of bonding forces than σ [51]. Studies have shown that for solids with central forces, the lower limit of σ is 0.25, and the upper limit is 0.5 [52]. Based on the obtained calculations, XAlSiH materials (X = Sr, Ca, and Ba) have strong central bonding. There is agreement in the B values when the compressibility moduli produced from C_{ij} and those from equations of state (EOS) are compared using the GGA approach. The C_{ij} computations accuracy can be better understood by looking at the correlation between the B values produced from C_{ij} and EOS.

Thermal conductivity tests can be used to predict phase transitions [53]. In the Debye model, thermal conductivity parameters are directly correlated with specific heat, which may be determined using the Debye temperature. The Debye temperature [46] is intimately associated with various physical properties of materials, including specific heat, elastic constants, and melting points. Acoustic vibrations are the main driving force behind vibrational excitations at low temperatures. By utilizing elastic constants, it is feasible to approximate the Debye temperature instead of quantifying low-temperature specific heat. The Debye temperature (θ_D) can be determined by calculating the average sound velocity, v_m, which is obtained by calculating the longitudinal (v_l)

Table 6. Modules of elasticity for XAlSiH (X = Sr, Ca, Ba) using GGA.

	SrAlSiH	CaAlSiH	BaAlSiH
B_V (GPa)	66.464	68.741	58.765
B_R (GPa)	62.472	61.960	56.425
B_H (GPa)	64.468	65.350	57.595
G_V (GPa)	54.028	54.805	49.909
G_R(GPa)	51.811	51.377	48.383
G_H (GPa)	52.919	53.091	49.146
E_V (GPa)	127.528	129.894	116.691
E_R (GPa)	121.769	120.754	112.883
E_H (GPa)	124.650	125.332	114.788
σ_V	0.180	0,185	0.169
σ_R	0.175	0,175	0.166
σ_H	0.177	0,180	0.167
B_H/G_H	1.2182	1.2309	1.1719
A_B %	3.0961	5.1881	2.0314
A_G %	2.0946	3.2284	1.5525
A^u	0.2778	0.4430	0.1991

and transverse (v_t) elastic velocities. The GGA method was used to calculate the values of the parameters for XAlSiH (X = Sr, Ca, and Ba) at zero pressure. These derived values are presented in table 7. Longitudinal elastic compression waves have a higher propagation speed compared to transverse elastic shear waves.

Based on the achieved results, CaAlSiH demonstrates a higher theoretical Debye temperature compared to the compounds SrAlSiH and BaAlSiH, suggesting increased resistance of CaAlSiH in comparison to XAlSiH (X = Sr, Ba). This temperature discrepancy also implies that CaAlSiH is more challenging to break than SrAlSiH and BaAlSiH. In solids, the T_D serves as an indicator of interatomic strength; thus, a higher Debye temperature signifies a robust bond between CaAlSiH and BaAlSiH and their surroundings. θ_D is known to exhibit an inverse relationship with molecule weight and can serve as a measure of the force of the covalent bonds in materials [54]. A correspondence is noted between the θ_D values calculated directly from C_{ij} and those estimated using the Gibbs2 code. This alignment enhances our confidence in the reliability of our findings.

The presence of elastic anisotropy in crystals can have a substantial impact on various physical processes, including anisotropic plastic deformation, fracture behavior, and elastic instability. Hence, it is imperative to compute the elastic anisotropy of structural hydrides in order to improve their mechanical resilience in mobile applications, including hydrogen storage [46]. To evaluate this anisotropy, one approach is to measure the extent of anisotropy in the atomic bonding across different planes by the computation of anisotropic shear factors. The parameters can be expressed in terms of a hexagonal material using the equations [55].

$$A_1 = 4C_{44}/(C_{11} + C_{33} - 2C_{13}) \tag{24}$$

$$A_2 = 2C_{66}/(C_{11} - C_{12}) \tag{25}$$

The shear anisotropy factors are A_1 in the {100} plane and A_2 in the {001} plane.

The shear anisotropic factors that have been determined are displayed in table 5. Elastic anisotropy is indicated by the deviation of the anisotropy factors from unity. The values of A_1 in our example are roughly 0.8972, 0.9568, and 0.7764 for SrAlSiH, BaAlSiH, and CaAlSiH, respectively, while A_2 is equal to 1 for all three compounds, using the GGA approximation (table 5). The findings indicate that XAlSiH compounds have significant shear anisotropy within the {100} plane, while our compounds demonstrate an isotropic shear modulus within the {001} plane.

The second method involves determining the percentage of elastic anisotropy in compression (A_B) and in shear (A_G), defined as follows. [46]:

$$A_B = (B_V - B_R)/(B_V + B_R) \times 100 \tag{26}$$

$$A_G = (G_V - G_R)/(G_V + G_R) \times 100 \tag{27}$$

The elastic anisotropy measures A_B and A_G quantify the material's elastic property variations with direction. A_B compares bulk moduli from Voigt and Reuss models, indicating bulk modulus anisotropy. Similarly, A_G compares shear moduli from these models, showing shear modulus anisotropy. These measures provide insights into the material's intrinsic anisotropic behavior, originating from its crystalline structure and microstructural arrangement. Anisotropy in bulk and shear moduli arises due to directional variations in stiffness caused by preferential bonding directions or crystal orientations. A_B and A_G reflect how these elastic properties deviate from isotropy, offering valuable insights into the material's mechanical behavior [46].

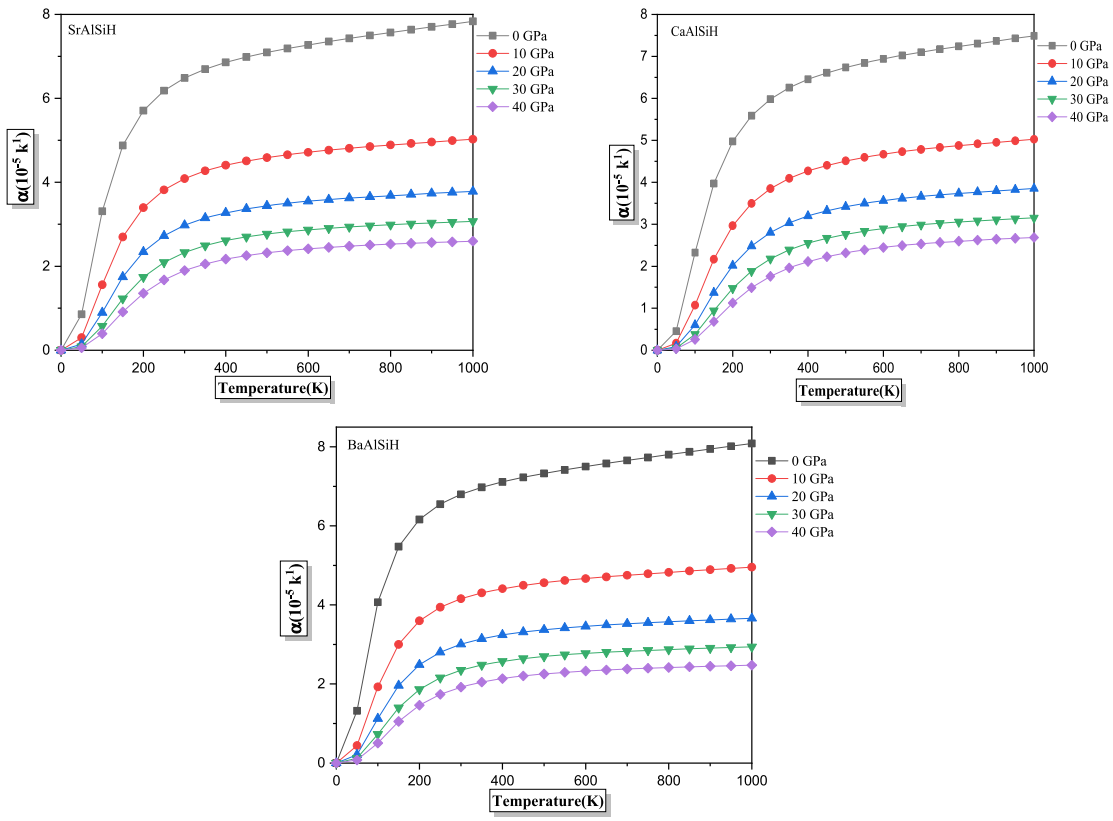

Figure 11. Variation of thermal expansion α of XAlSiH (X = Sr, Ca, Ba) compounds as a function of temperature investigated at different pressures calculated by GGA.

Table 7. Longitudinal, transversal, and average sound velocity values (v_l,v_t, v_m in m/s), temperature of Debye (θ_D in K) for XAlSiH (X = Sr, Ca, Ba) using GGA.

Compounds	ν_t	ν_l	ν_m	θ_D
SrAlSiH	4048.46	6466.87	4458.98	502.165
CaAlSiH	4756.12	7616.09	5239.81	606.615
BaAlSiH	3536.85	5598.11	3891.54	423.773

The bulk modulus, defined as B = −V (dP/dV), may not inherently imply anisotropy. However, directional variations in stiffness due to the material's microstructural arrangement and crystalline structure can result in anisotropic behavior. These variations influence the material's response to volume changes under stress, leading to differences in the bulk modulus along various crystallographic directions. Therefore, anisotropy in the bulk modulus arises from the inherent anisotropic nature of the material's structure and bonding configurations.

The values of A_B and A_G are zero for isotropic materials in terms of elasticity. The non-zero value of A_B (A_G) demonstrates the existence of elastic anisotropy under compression (shear) conditions. When $A_B = A_G = 100\%$, this corresponds to the maximum conceivable anisotropy. The GGA method was used to determine the anisotropy rates of volume and shear for the XAlSiH compounds (X = Sr, Ca, and Ba). The estimated rates for A_B are approximately 3.0961%, 5.1881% and 2.0314% for SrAlSiH, CaAlSiH, and BaAlSiH, respectively. The estimated rates for A_G are approximately 2.0946%, 3.2284%, and 1.5525% for SrAlSiH, CaAlSiH, and BaAlSiH, respectively (see table 6). In conclusion, these compounds exhibit a moderate degree of shear modulus anisotropy and bulk modulus anisotropy (compression). Additionally, it is observed that CaAlSiH displays a higher anisotropic bulk and shear modulus compared to SrAlSiH and BaAlSiH.

The third method involves calculating the universal index, which is defined as follows [56]:

$$A^U = 5\frac{G_V}{G_R} + \frac{B_V}{B_R} - 6 \tag{28}$$

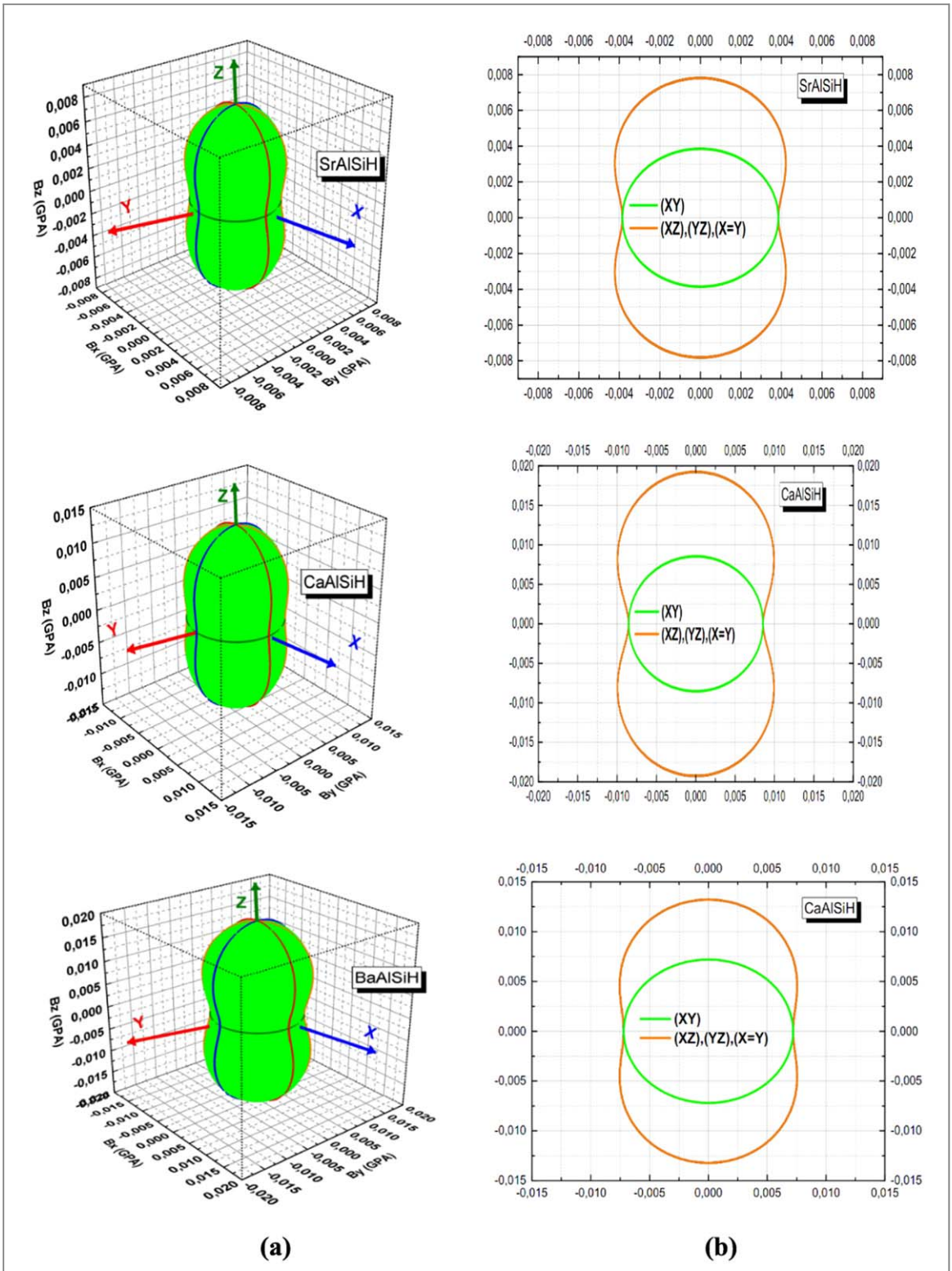

Figure 12. (a) Represent the orientation-dependent linear compressibility for SrAlSiH, CaAlSiH and BaAlSiH respectively. (b) represent their linear compressibility projections in different planes.

When A^U is equal to zero, it indicates isotropic elasticity of the material; and when A^U deviates from zero, it indicates anisotropic elasticity. According to the results in table 6, A^U is approximately 0.2778, 0.4430, and 0.1991 for SrAlSiH, CaAlSiH, and BaAlSiH, respectively, using the GGA method. All three materials demonstrate significant differences in elasticity depending on the direction of measurement. The elastic anisotropy index is mostly associated with the bulk and shear moduli [57, 58].

The aforementioned research lacks the necessary depth to precisely determine the elastic properties of a crystal. When building surface structures, it is recommended to use linear compressibility and the inverse of the modulus of

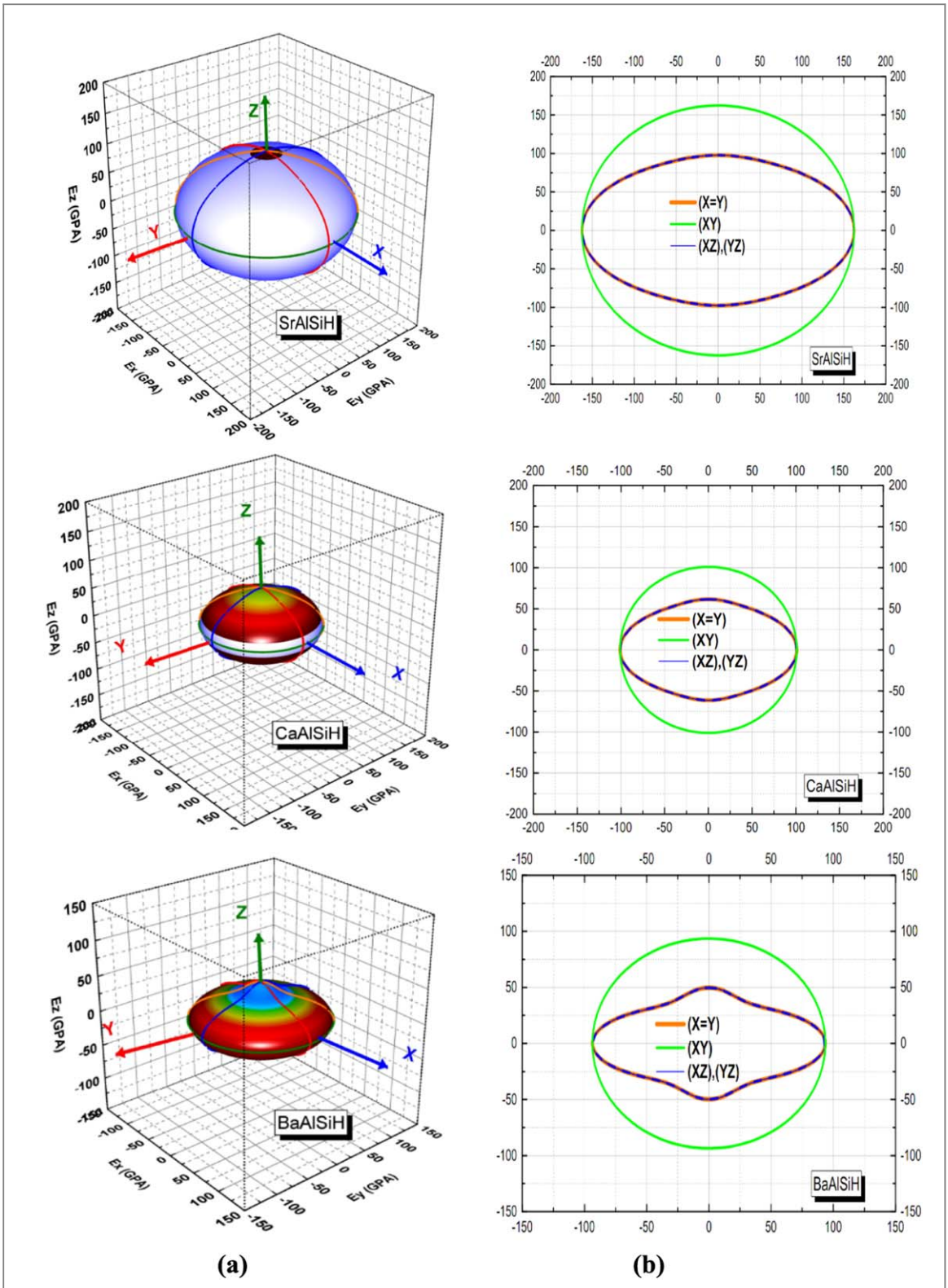

Figure 13. (a) Represent the 3D surface of the Young's modulus for SrAlSiH, CaAlSiH and BaAlSiH, (b) their cross sections in different planes respectively.

Young in different orientations. The following is illustrated by hexagonal systems in terms of linear compressibility:

$$\beta = (S_{11} + S_{12} + S_{13}) - n_2^3(S_{11} + S_{12} - S_{13} - S_{33}) \tag{29}$$

S_{ij} represent the deformability elastic constants and $n_1,\ n_2,\ n_3$: are the directional cosines (in spherical coordinates) following x, y and z respectively. The relations between the S_{ij} constants and the elastic constants C_{ij} is as follows [58]:

$$\begin{cases} S_{11} = 1/C_{11} \\ S_{33} = 1/C_{33} \\ S_{12} = S_{21} = -C_{12}/(C_{11}C_{22}) \\ S_{13} = S_{31} = -C_{13}/(C_{11}C_{33}) \\ S_{44} = 1/C_{44} \end{cases} \tag{30}$$

These relations allow for the conversion between stiffness and compliance properties of materials.

In equation (29), the linear compressibility β describes the material's response to volume changes under an applied stress. The equation relates β to the components of the compliance tensor S_{ij} and the direction n_2^3. The term $(S_{11} + S_{12} + S_{13})$ represents the sum of the compliance tensor components corresponding to the volumetric strain in the n direction. The term $n_2^3(S_{11} + S_{12} - S_{13} - S_{33})$ accounts for the anisotropic contributions to the compressibility, where the components S_{11}, S_{12}, S_{13} and S_{33} represent the material's response to stresses in different directions.

The expression that expresses Young's modulus E in the hexagonal system is its reciprocal along the direction of the unit vector n_i [58]:

$$E = \frac{1}{(1 - n_3^2)^2 S_{11} + n_3^4 S_{33} + n_3^2(1 - n_3^2)(2S_{13} + S_{44})} \tag{31}$$

Equation (31) measures the material's stiffness along a specific direction. The equation is a function of the compliance tensor S_{ij} and the direction n_3. The first term $\frac{1}{(1 - n_3^2)^2} \times S_{11}$ represents the contribution to E due to the material's response to tension or compression along the n_3 direction. The term $n_3^4 S_{33}$ accounts for the anisotropic contributions to E, where S_{33} represents the material's response to stresses in the n_3 direction. Finally, the term $n_3^2(1 - n_3^2)(2S_{13} + S_{44})$ captures the effects of shear stresses and their interaction with tensile or compressive stresses along n_3. These equations provide insights into the material's mechanical behavior, including its response to stress and its stiffness along different directions, offering valuable information for engineering and material science applications.

Figure 12 displays the calculated linear compressibility values derived from the theoretical elastic constants for SrAlSiH, CaAlSiH, and BaAlSiH. Equation (29) defines a three-dimensional surface where the distance from the origin of coordinates to the surface is equal to the linear compressibility in a certain direction. The cubic system exhibits isotropic linear compressibility, leading to a spherical shape. The absence of a spherical shape in figure 12 indicates that linear compressibility does not exhibit isotropy. The elastic anisotropy is greater in the (X = Y), (XZ), and (YZ) planes compared to the (XY) plane. Additionally, the linear compressibility in the (XY) plane is isotropic.

Figure 13 shows the projected orientation-dependent Young's modulus for SrAlSiH, CaAlSiH, and BaAlSiH using the elastic compliance constants. Equation (31) specifies a three-dimensional closed surface, where the distance from the origin of coordinates to the surface is equal to the Young's modulus in a specific direction. In a fully isotropic system, this surface would assume a spherical shape. However, this is not the case, even in a cubic system. The Young's modulus surface for the three compounds exhibits a nearly spherical shape. Consequently, these three compounds display a minimal level of anisotropy. The elastic anisotropy is higher in the (X = Y), (XZ), and (YZ) planes compared to the (XY) plane. Additionally, the elastic anisotropy is the same in the (X = Y) plane as it is in the (XZ) and (YZ) planes. Furthermore, the Young's modulus in the (XY) plane exhibits isotropy.

4. Conclusion

The study extensively explored hexagonal phase hydrides XAlSiH (X = Sr, Ca, and Ba) through the FP-LAPW approach based on Density Functional Theory (DFT), with a summarised outcome. We found the equilibrium structural parameters (a, c, and c/a) of XAlSiH compounds (where X can be Sr, Ca, or Ba). The lattice constants went up from CaAlSiH to SrAlSiH to BaAlSiH. The compounds' soft nature was attributed to a high degree of ionic character in chemical bonding. Electronic Characteristics: Electronic band spectra and total Density of States (DOS) indicated that XAlSiH (X = Sr, Ca, and Ba) compounds are semiconductors with an indirect bandgap ranging between 0.2 and 0.7 eV using the GGA and LDA approximations. Regarding the mBJ-GGA and mBJ-LDA approximations, the values range between 0.7 and 1.2 eV. Most elastic and thermodynamic parameters were explored for the first time, predicting further experimental and theoretical studies. Using the quasi-harmonic Debye model, first-principles calculations on XAlSiH (X = Sr, Ca, and Ba) compounds gave accurate results for how pressure and temperature change. The bulk modulus increased with pressure and decreased with temperature, impacting the decomposition temperature. Low bulk moduli suggested high compressibility of XAlSiH (X = Sr, Ca, and Ba), with gravimetric hydrogen storage capacities determined for BaAlSiH, SrAlSiH, and CaAlSiH at 0.52%, 0.71%, and 1.05%, respectively. Hydrogen desorption temperatures

were measured at 748.90 K, 311.57 K, and 685.40 K for these compounds. In the hexagonal structure, C_{11} exceeded C_{33}, indicating ready compressibility in the [001] direction compared to [100]. C_{44} was smaller than C_{11}, indicating a reduced ability to withstand shear deformation when compared to unidirectional compression. XAlSiH (X = Sr, Ca, and Ba) compounds were identified as fragile materials with significant volume changes during uniaxial deformation. Estimated Debye temperatures for SrAlSiH, CaAlSiH, and BaAlSiH were 502.16 K, 606.61 K, and 423.77 K, respectively. The study discovered that compounds of XAlSiH with a hexagonal structure exhibit isotropy in Young's modulus and anisotropy in bulk modulus. The meticulous and all-encompassing computations facilitate the production of scalable, multifunctional mechanical and thermal devices with exceptional performance.

Acknowledgments

The authors (H Ammi, T Ghellab, Z Charifi and H Baaziz) would like to thank the general directorate for scientific research and technological development for their financial support during the realization of this work.

Data availability statement

All data that support the findings of this study are included within the article (and any supplementary files).

ORCID iDs

Z Charifi https://orcid.org/0000-0003-3875-4716
H Baaziz https://orcid.org/0000-0003-4860-2740

References

[1] Mohamed A-B A, Khalil E M, Yassen M F and Eleuch H 2021 *Solid State Commun.* **336** 114383
[2] Cardoso G L, Piquini P C, Khossossi N and Ahuja R 2021 *Int. J. Hydrog. Energy* **46** 20586
[3] Asanova S M, Safaraliev M K, Kokin S E, Dmitriev S A, Arfan K, Zhabudaev T Z and Satarkulov T K 2021 *Int. J. Hydrog. Energy* **46** 34542
[4] Zhang Y, Zhang L, Pan H, Wang H and Li Q 2021 *Appl. Surf. Sci.* **535** 147683
[5] Pluengphon P, Tsuppayakorn-aek P, Sukmas W, Inceesungvorn B and Bovornratanaraks T 2021 *Int. J. Hydrog. Energy* **46** 22591
[6] Pang M-B, Hong S-I, Ri S-I and Kim J-C 2021 *Int. J. Hydrog. Energy* **46** 11824
[7] Chen S and Pan Y 2021 *J. Phys. Chem. C* **125** 11848–56
[8] Panwar K and Srivastava S 2021 *Int. J. Hydrog. Energy* **46** 10819
[9] Kojima Y and Yamaguchi M 2021 *Int. J. Hydrog. Energy* **46** 2306
[10] Vajeeston P, Ravindran P, Kjekshus A and Fjellvag H 2004 *Appl. Phys. Lett.* **84** 34
[11] Khowash P K, Rao K, McMullen T and Jena P 1997 *Phys. Rev.* B **55** 1454
[12] Karazhanov S Z, Ulyashin A G, Ravindran P and Vajeeston. P 2008 *EPL* **82** 17006
[13] Yvon K and Fischer P 1988 Hydrogen in intermetallic compounds ed L Schlapbach *Top. Appl. Phys.* 63, 87(Springer)
[14] Lee M H *et al* 2008 Crystal structure, electronic structure, and vibrational properties of MAlSiH (M = Ca,Sr,Ba): Hydrogenation-induced semiconductors from the AlB2 -type alloys MAlSi *Phys. Rev. B - Condens. Matter Mater. Phys.* **78** 1–11
[15] Blaha P, Schwarz K, Madsen G K H, Kvasnicka D and Luitz J 2001 *WIEN2k, an Augmented Plane Wave Plus Local Orbitals Program for Calculating Crystal Properties* (Vienna University of Technology)
[16] Perdew J P, Burke K and Ernzerhof M 1996 *Phys. Rev. Lett.* **77** 3865
[17] Otero-de-la-Roza A, Abbasi-Pérez D and Luaña V 2011 *Comput. Phys. Commun.* **182** 2232
[18] Otero-de-la-Roza A and Luaña V 2011 *Comput. Phys. Commun.* **182** 1708
[19] Blanco M A, Francisco E and Luaña V 2004 *Comput. Phys. Commun.* **158** 57
[20] Maradudin A A, Montroll E W, Weiss G H and Ipatova I P 1971 (Academic Press)
[21] Girifalco L A 2000 (Oxfort University Press) 62
[22] Jamal M *et al* 2018 IRelast package *J. Alloys Compd.* **735** 569–79
[23] Lee M H, Björling T, Hauback B, Utsumi T, Moser D, Bull D, Noreus D, Sankey O F and Häussermann U Crystal structure, electronic structure, and vibrational properties of MAlSiH (M = Ca,Sr, Ba): Hydrogenation-induced semiconductors from the AlB_2
[24] Björling T, Noreus D, Jansson K, Andersson M, Leonova E, Eden M, Hålenius U and Häussermann U 2005 SrAlSiH: A Polyanionic Semiconductor Hydride *Angewandte Chemie Internationale Edition* **44** 7269–73
[25] Björling T 2008 *Synthesis and Characterisation of Zintl Hydrides* 20
[26] Austin J 2009 *Supporting Information for the Manuscript* 1–42
[27] Utsumi T 2008 'AeAlSiH (Ae = Ca , Sr and Ba) Novel Semiconducting Zintl Phase Hydrides with Tuneable Band Gaps and Strong Metal–H Bonds,'
[28] Murnaghan F D 1944 *Proc. Nat. Acad. Sci. USA* **30** 244
[29] Sichla T and Jacobs H 1996 *Eur. J. Solid State Inorg. Chem.* **33** 453
[30] Bronger W, Chi C S and Mueller P 1987 *Z. Anorg. Allg. Chem.* **545** 69
[31] Brehm J A 2018 Predicted bulk photovoltaic effect in hydrogenated Zintl compounds *J. Mater. Chem. C* **6** 1470–5
[32] Björling T, Noréus D, Jansson K, Andersson M, Leonova E, Edén M, Hålenius U and Häussermann U 2005 *Angew. Chem. Int. Ed.* **44** 7269
[33] Christman J R 1988 *Fundamentals of Solid State Physics* (Wiley)

[34] Debye P 1912 *Ann. Phys.* **39** 789
[35] Anderson O L and Zou K 1989 *Phys. Chem. Miner.* **16** 642
[36] Broom D P 2011 *Hydrogen Storage Materials : The Characterisation of Their Storage Properties* (Springer)
[37] Klotz I M and Rosenberg R M 2000 *Chemical Thermodynamics. Basic Theory and Methods* 6th ed (Wiley Interscience)
[38] Chernyshov D, Bosak A, Dmitriev V, Filinchuk Y and Hagemann H 2008 *Phys. Rev. B* **78** 172104
[39] Fine M E, Brown L D and Marcus H L 1984 *Scripta Metall.* **18** 951
[40] Ghellab T, Charifi Z, Baaziz H, Latteli H, Güler M, Uğur Ş, Güler E and Uğur G 2022 *Physica B* **638** 413851
[41] Ghellab T, Charifi Z, Baaziz H, Telfah A, Ababneh R, Alsaad A and Sabirianov R 2022 *Solid State Commun.* **347** 114731
[42] Hill R 1952 *Proc. Phys. Soc.* **65** 349
[43] Hill R 1963 *J. Mech. Phys. Solid.* **11** 357
[44] Voigt W 1928 *Lehrbuch der Kristallphysik*
[45] Reuss A 1929 *Z. Angew. Math. Mech.* **9** 49
[46] Ravindran P, Fast L, Korzhavyi P A and Johansson B 1998 *J. Appl. Phys.* **84** 4891
[47] Caputo R and Tekin A 2011 *J. Sol. Stat. Chem.* **184** 1622
[48] Wills J M, Eriksson O, Soderlind P and Boring A M 1992 *Phys. Rev. Lett.* **68** 2802
[49] Nakamura M 1994 ed J H Westbrook and R L Fleischer *Intermetallic Compound: Principles* 1 (Wiley) 873
[50] Pugh S F 1954 *Phil. Mag.* **45** 823
[51] Bogdanovic B, Brand R A, Marjanovic A, Schwickardi M and Tolle J *J. Alloys.*
[52] Gross K J, Thomas G J and Jensen C M 2002 *J. Alloys Compd.* **330** 683
[53] Sundqvist B and Andersson O 2006 *Phys. Rev. B* **73** 092102
[54] Zhang X D, Hou Z F, Jiang Z Y and Hou Y Q 2011 *Physica B* **406** 2196–9
[55] Al-Ghaferi A, Müllner P, Heinrich H, Kostorz G and Wiezorek J M K 2006 *Acta Mater.* **54** 881–9
[56] Ranganathan S I and Ostoja-Starzewski M 2008 *Phys. Rev. Lett.* **101** 55504 No Title
[57] Kong Z, Duan Y, Qu D, Bao L and Peng M 2022 *Physica B: Phys. Condens. Matter* **624** 413371
[58] Yang A, Duan Y, Yi J and Li C 2021 *Chem. Phys. Lett.* **783** 139088
[59] Imai M, Nishida K, Kimura T and Abe H 2002 *Appl. Phys. Lett.* **80** 1019
[60] Lorenz B, Lenzi J, Cmaidalka J, Meng R L, Sun Y Y, Xue Y Y and Chu C W 2002 *Physica C* **383** 191
[61] Bogdanovic B and Schwickardi M 1997 *J. Alloys Compd.* **253** 1
[62] Lauher J W, Dougherty D and Herey P J 1979 *Acta Cryst.* **B35** 1454
[63] Lorenz P R B, Cmaidalka J, Meng R L and Chu C W 2003 and014512 B 68
[64] Giantomassi M, Boeri L and Bachelet G B 2005 *Phys. Rev. B* **72** 224512
[65] Meng R L, Lorenz B, Wang Y S, Cmaidalka J, Sun Y Y, Xue Y Y, Meen J K and Chu C W 2003 *IEEE Trans. Appl. Supercond.* **13** 3042
[66] Nakagawa T, Tokunaga M and Tamegai T 2006 *Sci. Technol. Adv. Mater.* **7** S108